Journal of *Marine Science and Engineering*

MDPI

Article

Thrust Enhancement of DTMB 5415 with Elastic Flapping Foil in Regular Head Waves

Lei Mei [1], Wenhui Yan [2], Junwei Zhou [1,*] and Weichao Shi [3]

[1] School of Ocean Engineering, Harbin Institute of Technology (Weihai), Weihai 264209, China
[2] School of Mechanical and Material Engineering, North China University of Technology, No. 5 Jinyuanzhuang Road, Beijing 100144, China
[3] Department of Naval Architecture, Ocean and Marine Engineering, Strathclyde University, Glasgow G4 0LZ, UK
* Correspondence: zhoujunwei@hit.edu.cn; Tel.: +86-133-5681-6816

Abstract: Recent studies indicate that bow foil biomimetic systems can significantly improve ship propulsion in waves. In this paper, the DTMB 5415 ship model is taken as the object and a semi-active elastic flapping foil is proposed to install at its bow underwater position. When a ship sails in head wave, heave and pitch motion will occur, which will drive the bow foil to form heave motion. According to the working characteristics of elastic foil, bow foil can generate forward thrust under drive of given heave motion. At first, co-simulation of the ship with self-pitching bow foil in head waves is realized by ISIS-CFD solver and preliminarily realizes drag reduction and thrust increase effect of the bow foil. At the same time, it is found that the effect of bow foil on hull drag reduction is reflected in two aspects, one is the additional thrust generated by the bow foil and the other is that suppression of the bow foil on hull motion also reduces hull resistance in waves. Then, in order to optimize the working characteristics of elastic bow foil, the influence of spring stiffness and span length of the bow foil on drag reduction and thrust increase effect is discussed. A preliminary spring optimization result is obtained, as well as the influence of the span length of the bow foil on the system.

Keywords: thrust enhancement; resistance reduction; elastic flapping foil; regular wave; torsion spring stiffness

Citation: Mei, L.; Yan, W.; Zhou, J.; Shi, W. Thrust Enhancement of DTMB 5415 with Elastic Flapping Foil in Regular Head Waves. *J. Mar. Sci. Eng.* **2023**, *11*, 632. https://doi.org/10.3390/jmse11030632

Academic Editor: Md Jahir Rizvi

Received: 15 February 2023
Revised: 13 March 2023
Accepted: 14 March 2023
Published: 17 March 2023

1. Introduction

1.1. Background

In real sea conditions, marine craft experience undesirable wave-induced oscillatory, heave, and pitch motions. These will affect the stability of ships [1] and increase ships' resistance in navigation [2,3]. Historically, foils have been investigated either as anti-pitching fins on ships [4–6] or for propulsion in a wavy flow [7–11]. In the 1980s, researchers combined these topics to specifically investigate the effect of bow foils on ship motions and propulsive efficiency. Bow foils are streamlined hydrofoil fins connected to the bow area of the hull. Foils can be fixed or pivoting depending on hull motion due to waves. In this case, the ship motions, especially heaving and pitching, could be exploited for providing foil's heaving oscillatory motion free of cost [12,13]. The wave-induced flapping motion of submerged flapping foils combined with incident wavy flow results in a time-average thrust force. This thrust can be used to augment the existing propulsion [14,15], significantly reducing fuel consumption, or used as the primary propulsion [16], eliminating the necessity to carry propulsive energy reserves for entire journeys. Additionally, the device can contribute to damping the hull motions, improving operability [17].

1.2. Investigations Regarding Bow Foil

Use of bow foil for propulsion is not a new concept. The initial attempts of wave-augmented propulsion were first demonstrated almost 120 years ago through a series of full-scale trials of a 13 ft boat with flapping foils mounted at the bow and stern [18]. However, they were only reported as interesting ideas rather than academic studies. Wave-augmented propulsion boats did not receive significant attention until the 1970s when Jakobsen started a series of model experiments and full-scale trials. In 1981, Jakobsen designed a spring-attached foil propulsion system, generating thrust due to ship motions relative to the water, and conducted a series of model experiments and full-scale trials. The foil propulsion system reportedly was able to save 30% of fuel in headwind waves at a speed of 6 kn [12]. In parallel to the developments in Europe, Isshiki in Japan investigated a similar concept, experimentally mounting a bow foil on an 80 m cargo ship, thus demonstrating possibility of fuel economy [8–10]. Full-size trials in 1995 of a 174-ton Russian research fishing vessel not only confirmed potential savings in engine power but also revealed simultaneous moderation of longitudinal motions.

Increasing interest in the research community on the topic of bow foil system has been observed in the last two decades. According to the fixed mode, the bow foil wave-augmented propulsion system can be roughly divided into three kinds: fixed foil (does not have an adjustable angle of attack), semi-passive foil with spring-controlled pitch motion, and active pitch-controlled bow foil (foil's rotation about its pivot axis is actively controlled based on the history of its vertical oscillation). All the heaving motions of a bow foil system are provided by the ship motions.

At the first stage of research, use of semi-passive flapping foils for augmenting propulsion was considered in order to directly convert kinetic energy from ship motions to thrust and simultaneous ship motion reductions. In such cases, pitching motion of foils is induced by spring-loaded unsteady wing pressure distribution. Rozhdestvensky and Ryzhov [19] conducted a comprehensive review on the evolution of flapping propulsion design and on development results of vehicles equipped with them, analyzing the most common ones in terms of aerohydrodynamics and implementing some numerical models. Naito and Isshiki [20] reviewed various strategies for improved bow foil technologies (either fixed or passively controlled system). The effects of wing shape, size, position, and stiffness on the characteristics of thrust and resistance were detailed. Various control and energy conversion strategies were also discussed. In this direction, Terao [21] installed a passive dual-fin system at the stern of Suntory Mermaid II catamaran that sailed from Hawaii to Japan in 110 days empowered only with wave energy. Later, Terao and Sakagami [22] designed and developed a wave-powered boat with a similar system and conducted test tank and sea trials successfully, demonstrating its autonomous navigation performance. Bockmann & Steen [23] studied different pitch strategies for maximizing forward thrust. They demonstrated at model scale that fixed, passive, and active foil thrusters in waves can reduce resistance and heave and pitch motions when travelling at constant forward speed. However, the pitch motion of the spring-loaded foil is shown to produce higher thrust than that of the actively pitch-controlled foil tested. More recently, Bowker et al. [24,25] developed and experimentally validated a hybrid discrete time-domain numerical model from a prototype wave-propelled boat with flapping foils in regular head waves and determined change in forward speed due to unsteady thrust from passively sprung foils. In 2022, Zhang [15] proposed a wave foil with a passive angle of attack (AoA) adjustment with spring, where changes in AoA can promote extraction of energy from the waves. A model of heave and pitch motion with a wave foil was derived and the simulation carried out. The analysis showed that the proposed wave foil can extract wave energy to propel the ship and reduce the pitching motion of the ship.

With the in-depth research on the motion trajectory and active control of the flapping foil [26,27], the overall results suggest that actively oscillating foil systems in waves, under suitable conditions, have the possibility to recover the wave energy, rendering these systems applicable to marine unsteady thrusters. Numerous research studies began to focus on the

active-control bow foil augmentation system. Naito and Isshiki [20] proposed an actively pitch-controlled foil where the pressure at the bottom surface of the foil was used as an input in the control system. In the work by Belibassakis and Politis [28], the previous analysis has been extended to flapping foils coupled with ship motions, showing significant thrust development by extracting energy from the waves. They suggested to replace the passive spring-loaded rotation mechanism by simple actively controlled enforced pitch motion based on the (irregular) history of wing's vertical oscillation. They introduced a method for coupling of ship dynamics with unsteady flapping foil hydrodynamics by using linear seakeeping analysis in conjunction with unsteady lifting-line theory and non-linear 3-D panel methods. Next, in Belibassakis and Filippas [29] and Filippas [30], the boundary element method is extended to treat active pitch control of the flapping hydrofoil, taking into account the ship dynamics and effects of foil submergence and its horizontal location along the (forward part of the) ship, aiming at investigation of the performance of this active system in realistic sea states. Later, Huang et al. [31] proposed an Eco-Ship empowered with active flapping foils exploiting wave propulsion and studied that system experimentally with conduction free-running model tests, reporting speed improvement up to 6.24% and significant energy extraction. More recently, in Filippas et al. [32], in-house GPU-BEM and HPC-RANSE solvers were developed to further investigate the performance of active flapping foils propulsion for augmentation of ship prolusion, focusing on free-surface, irregular wave, and viscosity effects. Then, Kostas Belibassakis et al. [33] completed laboratory model testing of the bio-mimetic thruster with active control at the towing tank of National Technical University of Athens (NTUA) with ship hull models of specific type. The results showed that the additional thrust generated by the dynamic foil enabled the engine to operate in part-load without compromising vessel speed, resulting in an additional positive effect on the emission profile. In 2022, a novel BEM and high-performance GPU accelerated computational code have been exploited by Filippas and Belibassakis [32] for treatment of the nonlinear problem of lifting flows around foils beneath the free surface in obliquely incident waves and applied to hydrodynamic analysis of biomimetic thrusters with active control for augmenting ship propulsion in waves. The model has been further developed for simulation of active control system performance in head and quartering waves by them, including comparisons against detailed BEM and CFD predictions [32]. They also compared with the experimental results and further calibrated the thrust power coefficient diagram and expanded the prediction to a large-scale model to be tested at sea.

In addition, researchers also studied fixed bow foil wave-augmented systems [17,34,35] that do not have an adjustable AoA. Specifically, model-scale, towed resistance tests of a container ship and tanker with scale ratios of 1:57.7 and 1:16.57, respectively, have been conducted by Feng et al. [17] and Bockmann and Steen [17] to evaluate the effect of fixed bow foils on ship added resistance and motions in regular waves. Both studies achieved 60% reduction of resistance in waves, with additional reduction of 42% and 45% of hulls' heaving and pitching motions, respectively. In 2016, Bøckmann and co-workers founded the Wavefoil company, making a first attempt to generate a retractable version of the proposed system with fixed foils. During September of 2019, they installed a wave foil module on 40 m ferry M/F Teistin, achieving a 10% reduction to average fuel-oil consumption (http://wavefoil.com/ accessed on 13 March 2023). Huang et al. [31] presents experiments of a model container ship (R = 1:50), comparing the delivered power of an active pitch-oscillating bow fin to a fixed bow fi, over a range of speeds at two wave periods (equal to a wavelength to ship length ratio of 1.0 and 1.3). Although no comparison with and without the foil is given, the results indicate that pitching foils may outperform fixed foils. Bøckmann et al. [35] estimated the fuel savings for a general cargo ship employing retractable bow foils. They also demonstrated the importance of accurate thrust calculations in estimation of fuel savings, illustrating the necessity of CFD simulations.

To sum up, the research on the hydrodynamic problems of bow foil wave-augmented propulsion system has mainly focused on the following aspects:

First, numerical prediction on the coupling effect of hydrofoil and wave [9,26,36] includes the influence of a series of parameters; immersion depth of hydrofoil and free surface effects [32,36]; phase difference between waves and hydrofoil; size, location, geometry, and number of hydrofoils [20,34]; and oblique waves [33,34]. The research in this area is relatively mature and can be used as the basis for studying interaction and coupling between waves, oscillating foils, and hull.

Second, motion and force coupling of waves, hull, and hydrofoil: this problem involves coupled interaction between wave surface, hull, and hydrofoil and complex flow features that continuously change during maneuvering. The physical understanding of this complex flow is very important and essential for design purposes. Because of the expensive and complex computation of Navier–Stokes solver, a simple and common approach is to obtain the hydrodynamic force coefficients for the bare hull using a computer program based on 3-D panels with a distribution of potential flow singularities [37] or strip theory [24], add the separately calculated foil forces, and solve the equations of motions [17,28,29]. To date, it should be noted that the existing data (knowledge) base is still far from complete, and most of them are based on potential-based panel method or nonlinear boundary element methods, such as the series of work of Kostas Belibasakis and *Evangelos filippas* research group [28–30,32,33]. In Bøckmann's work, VeSim was used to simulate a ship with fixed bow foil, and a slightly modified version of the Leishman–Beddoes dynamic stall model was used to calculate the foil forces with two-way coupling between the ship motions and foil forces [17,35]. In 2021, based on quasi-steady lifting line theory in conjunction with unsteady thin hydrofoil theory, Bowker modeled the free-running response of a wave-propelled boat, capturing the coupled dynamics of the hull and foils, and a hybrid discrete time-domain numerical model was developed [24]. That is, although free-running experiments and in situ trials have been completed by some researchers, a coupled numerical model of hull with bow foil wave-augmented systems that could accurately capture the forward speed and dynamic response remains challenging. Much effort is needed for further development of physical and mathematical models to adequately describe the relevant processes, especially viscous and separated flow processes.

1.3. Paper Contribution and Outline

Compared with the boundary element method based on potential flow theory, CFD methods based on viscous flow (e.g., two-dimensionality (2-D)/3-D RANS and 3-D DES) have greater advantages for yielding more accurate and detailed results (such as separated vortices) for complex geometric and physical models, and it is easier to distinguish the continuously changing complex flow characteristics in the process of motion. With the sufficiently studied RANS viscous flow numerical method for hull motion [38–40] and hydrofoil hydrodynamic characteristics [23,41–46], the coupled motions and resistance in waves of a ship with bow foils can be found by using a Navier–Stokes solver in theory.

This paper presents a self-pitching bow foil wave-augmented propulsion system with passive AoA adjustment. It constructs a single degree of freedom spring-mass system in the direction around the pitching motion axis. The bow foil is located in deeper water below the bottom of the ship, which reduces free-surface effects [14,15] and increases protection in case of collision. In order to adequately describe the free-running response of a bow foil wave-augmented propulsion boat, especially coupled interaction, viscous, and separated flow processes, the effects of flow unsteadiness, 3-D, and non-uniformity of the oncoming flow (presence of large-scale vortex structures and wing–body interference effects), a novel co-simulation method is used to realize hydrodynamic and structure coupling of the hull, hydrofoil, and wave in this paper. Based on the ISIS-CFD solver of NUMECA software, coupled interaction between the bow foils and ship under head sea condition is modeled, the motion and total drag of a ship with bow foil is evaluated, and the influence of design parameters on system performance is further discussed.

The layout of this paper is as follows: Section 2 outlines the parameters of the proposed hull, foil, and wave conditions. Section 3 details the methodology, including the design of

the model, the fluid–structure coupling numerical method, and full validation. Section 4 systematically presents the co-simulation results. The effects of the spring stiffness ratio (k') and span length (h) of the bow foil on the drag reduction and thrust increasability of the system are also discussed, and the sensitivity of the performance to variation in several governing parameters is also evaluated in the current study. Finally, Section 5 summarizes the key insights obtained from the experimental study. The results provide a new dataset on wave augmented bow foils for a generic hull form, including co-simulation method, force coefficients, flapping parameters, and ship motion response.

2. Ship with Semi-Passive Flapping Foil in Head Wave

A sketch of a ship with semi-passive flapping foil in head wave is shown in Figure 1. The main particulars of the ship model (1/24.8 scale), airfoil model, and wave model are provided in Table 1. As shown in Figure 1, the ship with semi-passive flapping foil wave-augmented propulsion system refers to a self-pitching hydrofoil that is constrained by the torsion spring installed on the bow through the rotation axis. The rotation axis of the hydrofoil is located at the leading edge of the hydrofoil, and a virtual torsion spring is shown as the red spiral line at the leading edge of the hydrofoil in Figure 1. When the semi-passive flapping foil heaves under the drive of the hull in waves, the heave motion together with the advance velocity creates an oscillating hydrodynamic force and moment causing the foil to work at an angle of attack α. The torsion spring is used to restore the foil towards the equilibrium position. Under the combined action of this hydrodynamic moment and torsion spring, the flapping foil produces a pitching angle θ and generates thrust T_F.

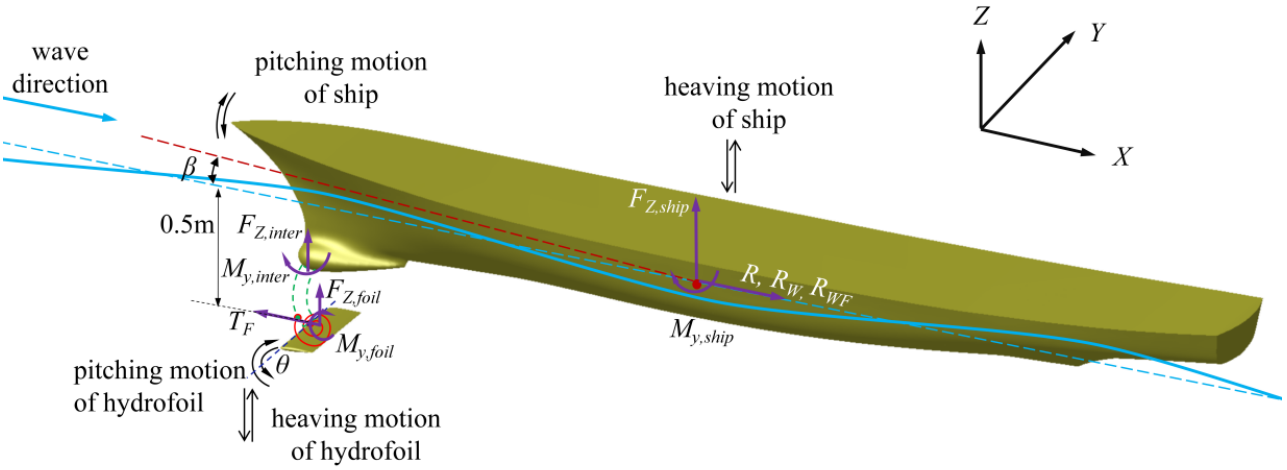

Figure 1. Frames of reference and sketch of the relationship between hull, flapping foil, and wave.

Table 1. Main particulars of DTMB 5415, NACA 0012 airfoil model, and waves.

Particulars		Value	Unit
Length at water level	L_{WL}	5.72	m
Breadth Overall	B	0.76	m
Draft	D	0.248	m
Volume	∇	0.549	m^3
Wetted surface	S_W	4.786	m^2
Airfoil Chord	c	0.2	m
Airfoil Span	h	0.4	m
Wave amplitude	A	0.05	m
Wave period	T	2.5	s
Wave length	λ	9.75	m
Wave height	H	0.1	m
Encounter angle of wave		180	○

The well-known benchmark naval hull form DTMB 5415 is used as the ship model in this paper. A rigid three-dimensional NACA 0012 airfoil with a chord length, c, and a foil span, h is used, and its horizontal projection is approximately rectangular. The 3-D flapping hydrofoil model is designed with equal chord length. Round corners are designed at both ends of the span direction of the flapping hydrofoil, with a radius of R = 0.1 c, and connected with an elliptic curve to form the end shape. The foil is installed at a deep position below the bow through a virtual support (as shown by the green dotted line between the bow and the flapping foil in Figure 1) 0.5 m below the still water surface. We consider the ship traveling at constant forward speed V in basic waves propagating at a 180 deg angle with respect to the ship longitudinal axis, which corresponds to head incident waves. The wave is a second-order Stokes wave based on VOF model, defined by

$$\zeta(t) = \frac{H}{2}\cos(Kx + \omega t) + \frac{\pi H}{4}\frac{H}{\lambda}\cos 2(Kx + \omega t) \quad (1)$$

where K is the wave number; λ is wavelength, m; H is wave height, m; and ω is the wave frequency.

When the ship sails against the waves at different speeds, the period and frequency of the waves it encounters are different. For the flapping foil, the encounter frequency f_e is its working frequency, which is very important to its hydrodynamic performance. The encountering frequency is expressed as

$$f_e = \frac{C_w + V}{\lambda} \quad (2)$$

where C_w is wave velocity, m/s; λ is wavelength, m.

In order to more clearly show the coupled interaction between the wave, hull, and flapping foil, this paper only discusses the system in typical sea states in head seas and ignores the influence of other wave factors. Therefore, only two degrees of freedom of heave and pitch motion are considered for both the hull and flapping foil. The hull heave and pitch motions were evaluated with respect to the fixed inertial frame of reference (oXYZ), as shown in Figure 1. The hull-induced foil heave motion was evaluated as a remote location on the hull at a depth below the waterline (0.5 m), and the pitch of the flapping foil (θ) was evaluated about the pivot point when the hull's pitch angle is β. The arrangement of the foil in the water below the bottom of the ship in this paper is intended to reduce the free-surface strong nonlinear effects on the flapping foil, and the selection of wave conditions in this paper is based on the possibility of generating waves in the laboratory and the ratio of wave length to ship length. That is, this condition could realize a strong wave response of the hull under the normal wave-making conditions in the laboratory [34], and it is near the optimum wavelength to length ratio, of approximately 1.25, for head waves [24]. A relatively small value is selected for the wave height, the purpose of which is to study whether there is still an obvious wave-augmented propulsion effect under the condition of small-amplitude waves.

The motion equation considering the interaction between the hull/the flapping foil and the fluid and the interaction between the hull and the flapping foil will be automatically solved by ISIS-CFD solver in NUMECA software. The equations of heaving, pitching motion of the hull, and pitching motion of the flapping foil are listed in Equation (3). The relationship between the parameters in Equation (3) can also be viewed in Figure 1. In order to understand the relationship between the parameters, the formulas in Equation (3) are simplified. That is to say, considering the slow and small pitch motion of the hull, its influence on the heave force on the hull is ignored (assuming that the center of inertia moment coincides with the hull centroid). The influence of hull pitch motion on the movement of the flapping foil in the X direction and the influence of the X direction force between the flapping foil and the hull on the ship's pitch motion are also ignored. However, in the actual simulation, the software takes these factors into account. The influence of

the attached water of the hull and the flapping foil is also estimated by the solver in each iteration.

$$\begin{aligned} m_{ship}\ddot{z} &= F_{z,ship} + F_{z,inter} \\ I_{ship}\ddot{\beta} &= M_{y,ship} + M_{y,inter} + F_{z,inter}L_{shaft} \\ I_{foil}\ddot{\theta} + k(\theta - \beta) &= M_{y,foil} \end{aligned} \tag{3}$$

where m_{ship} is the hull mass considering the attached water; I_{ship} is the pitch rotational inertia of the hull considering the attached water; I_{foil} is the pitch rotational inertia of the flapping foil considering the attached water; $\ddot{z}$ is the acceleration of hull shape center in Z direction, $\ddot{\beta}$ is the acceleration of hull pitching motion, θ and $\ddot{\theta}$ are the pitching angle and pitching motion acceleration of flapping foil; $F_{z,ship}$, $M_{Y,ship}$, and $M_{y,foil}$ are the forces and moments acting on the hull and hydrofoil (the effects of hydrostatic, wave and other factors are considered in the analysis; L_{shaft} is the distance from the flapping foil axis to the X coordinate of the hull centroid; $F_{z,inter}$ and $M_{y,inter}$ are the Z-direction force and Y-direction torque of the flapping foil on the hull ($M_{y,inter} = -k(\theta - \beta)$).

As shown in Figure 2, when the flapping foil propulsion is driven by the heave direction driven by the hull, the heave speed V_z is generated, and the forward speed V_x of the flapping foil is almost the same as the ship's speed V. Consequently, the heave motion together with the advance velocity will create an oscillating hydrodynamic force and moment causing the foil to work at an AoA α. Under the restraint of the torsion spring, it can work at a certain pitching angle θ.

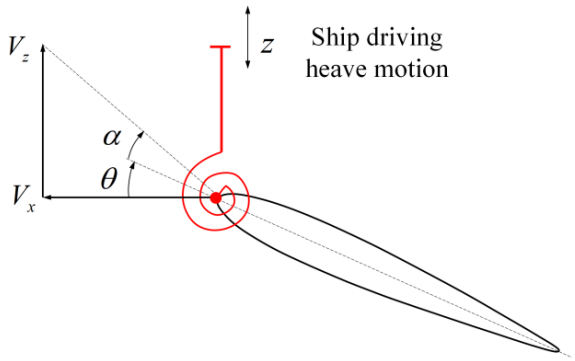

Figure 2. Schematic illustration of semi-passive flapping foil with forced heave motion and attached torsion spring.

According to previous studies, the AoA of the flapping foil, α, is one of the important parameters affecting the performance. As shown in Figure 2, if ignore the moving speed of the water particle in the wave, the AoA can be expressed as Equation (4):

$$\alpha(t) = \arctan\frac{V_z(t)}{V_x} - \theta(t) \tag{4}$$

The previous research results on semi-passive flapping foil propulsion show that the spring stiffness k and frequency ratio r are two important parameters that affect the system performance. The relationship between them can be expressed as follow Equation (5) [47]. In this paper, a fixed and sufficiently small rotational inertia of the flapping foil = 001 kg·m^2 is selected for the research because, when the frequency ratio is small, that is, the foil has a small rotational inertia, the semi-passive flapping foil can work well, and the influence of rotational inertia on hydrodynamic force can be ignored. The effect of spring stiffness on propulsion performance and motion of wave-augmented propulsion system is mainly

discussed at a relatively lower rotational inertia of the flapping foil. The basic torsion spring stiffness is selected as $k = 20\ \mathrm{N} \times \mathrm{m/rad}$

$$r = \frac{f_e}{f_N} = 2\pi f \sqrt{\frac{I_{f0}}{k}} \tag{5}$$

where f_N is the natural frequency of the semi-passive flapping foil, Hz; f_e is the flapping frequency; I_{f0} is the inertia moment of the flapping foil without the attached water, kg·m^2.

3. Numerical Method

Based on the general-purpose ISIS-CFD solver of FINE/Marine, the rigid body dynamics equation and fluid hydrodynamic equation are solved simultaneously for coupled interaction between the bow foils and ship in head sea condition, and to verify that the proposed wave foil is capable of generating propelling forces. This solver adopts internal implicit iteration within a time step iteration to find the field of all hydrodynamic unknown quantities and ensure strong and accurate flow/motion coupling.

Flow solver ISIS-CFD is developed by CNRS/Centrale Nantes and distributed by Cadence-NUMECA as part of the FINE/Marine flow simulation suite. ISIS-CFD is an incompressible unsteady Navier–Stokes solver for multifluid flow based on the finite-volume method to build the spatial discretization of the transport equations [48,49]. The velocity field is obtained from the momentum conservation equations and the pressure field is extracted from the mass conservation constraint transformed into a pressure equation [50]. The solver ISIS-CFD adopts the second-order backward difference scheme in time format and the Gamma Differential Scheme [51] in space, which has two-order accuracy and high computational stability.

Free-surface flow is modeled with the two phase VOF approach with a interface tracking and interface- capturing method [52]. Both steady and unsteady free-surface flows are solved with a time integration technique. The solver is mostly used with unstructured hexahedral grids generated by the Hexpress grid generator, which can well adapt to complex geometric shapes [47]. The dynamic mesh technology can ensure the mesh quality after deformation.

3.1. Hydrodynamic Function

The hydrodynamic model uses the hull motion as its input to determine the hydrodynamic force and moment of the bow foil wave-augmented propulsion system. As for the dynamic model, the hydrodynamic force and moment from the hydrodynamic model are applied in the Newton–Euler equation to determine the foil and hull motion. By using Reynolds-averaged integral incompressible viscous fluid dynamics equation, considering the motion of grid cells and the influence of gravity, the continuity equation and momentum equation can be written as follows.

$$\frac{\partial}{\partial t}\int_{\Omega} \rho d\Omega + \oint_{S} \rho \vec{v} \cdot d\vec{S} = 0 \tag{6}$$

$$\frac{\partial}{\partial t}\int_{\Omega} \rho v_i d\Omega + \oint_{S} \rho v_i \vec{v} \cdot d\vec{S} = \oint_{S} \tau_{ij} dS_j - \oint_{S} p dS_i + \int_{\Omega} \rho g_i d\Omega \tag{7}$$

where Ω is the element volume; $\vec{v}$ is the flow velocity; v_i is velocity component; τ_{ij} is the sum of viscous stress and Reynolds stress and p is the pressure; S_j is the components of area vector and $\vec{S}$ is the area vector of element surface. g_i is the acceleration component of the element, which has a component only in the direction of gravity. The turbulent viscosity coefficient is determined by Menter's k-ω shear-stress transport turbulent model (Menter and Rumsey, 1994).

In order to capture the free liquid surface, the VOF (volume of fluid) method is used to define the volume fraction α', and the density is expressed as

$$\rho = \alpha'\rho_w + (1 - \alpha')\rho_\alpha \tag{8}$$

where, ρ_w and ρ_α are the densities of water and air, respectively.

3.2. Mesh and Method

The simulation is carried out in a numerical wave tank with a computational domain of 40 m wide, 60 m long, and 10 m deep. The height above the water surface is also 10 m. A numerical wave generator in front of the tank is given in the form of boundary condition. The bow of the ship is 10 m away from the wave generator, about 1 wavelength distance. A numerical wave absorber is set in the rear section of the tank, which is 20 m long and about two wavelengths away. After testing and observation, wave absorber can play a good role in wave elimination. The free surface is modeled with the two phase VOF approach with a high-resolution interface capturing (HRIC) scheme. One half of the calculation domain diagram is shown in Figure 3.

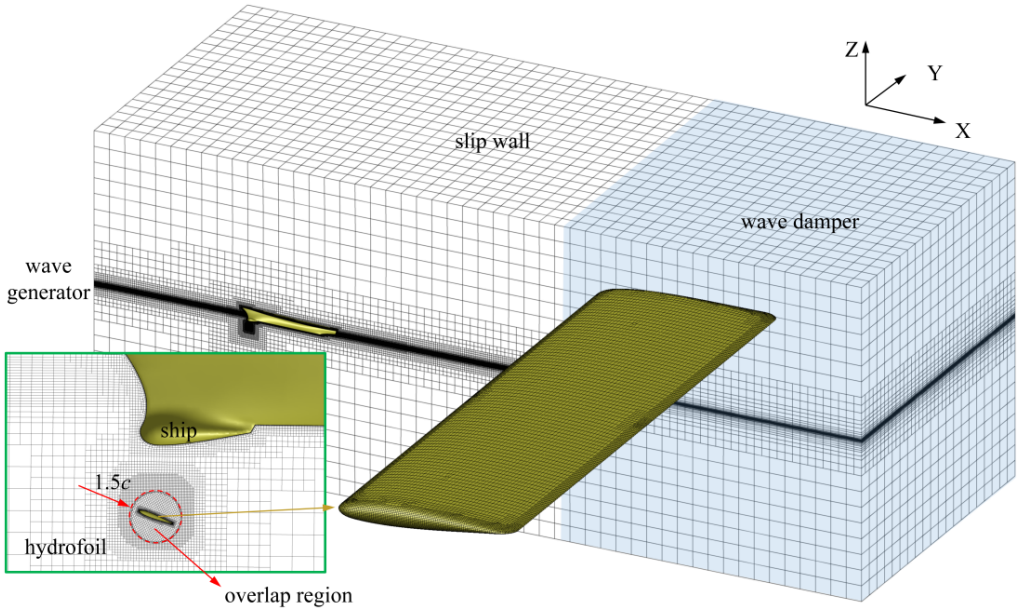

Figure 3. Schematic diagram of computational domain (one half of the calculation domain), boundary conditions, and local successive mesh refinement.

A multi-block dynamic overlap grid approach is adopted in the whole calculation domain to allow relative motion between the grids for hull motions, that is, the computational domain grid will produce elastic deformation with the heave and pitch motion of the hull. The grid motion velocity is hidden in the hydrodynamic equation, so the interpolation error caused by mesh deformation is avoided and the numerical accuracy is improved. In addition, in order to describe the motion of the semi-passive flapping foil propulsion accurately, the overlapping grid technique is used to construct the foil domain grid (overlap grid). The overlap grid subdomain around the foil is cylindrical, with a diameter of 1.5 c, which shown as red circular subdomain in Figure 3. The width of this cylinder in the Y direction is the sum of airfoil Span h and one airfoil chord c, that is, the width of the left and right sides is 0.5 c more than the airfoil Span h. The overlap grid subdomain around the foil makes rigid motion together with the foil.

The setting method of boundary conditions is shown in Figure 3. The entrance boundary of the calculation domain is determined by the wave generator, and the exit boundary is determined by the wave damper. The surfaces on both sides and the upper

and lower surfaces are set as slip wall boundary conditions. Both the hull surface and the hydrofoil surface are non-slip wall boundary conditions and numerical interpolation is used to transfer information at the interface of overlap grids region.

To reduce computation for the background mesh, a hexahedron mesh with local successive refinement method was chosen for the computational domain to keep just some local region as a refined mesh, as shown in Figure 3. In order to accurately simulate the changes of the wavefront around the hull and the separation and wake vortex of hydrofoil, mesh refinement is carried out on the free surface, hull and foil's surface, and in the ship wave region, respectively. The enlarged detail grid of the free surface and ship wave region is shown in Figure 4, which is the top view of local successive refinement of the grid near the free surface. As shown in Figure 4, the mesh of wave damper region is not refined, and the refined mesh sizes of the hull surface region, the parallel wave region, and the ship wave region are different. In addition, as can be seen from Figure 3, additional refinement is performed in the overlap grid region around the foil and the hydrofoil edge region. The refined mesh size of different regions are shown in Table 2, and the reference dimensions are wavelength λ, wave height H, and hydrofoil chord length c. The refined near-wall mesh could ensure the wall y+ value on the hydrofoil surface is about 1.0, and the wall function approach is used for the near wall treatment on the hull surface; the value of wall y+ on the hull surface is about 10.

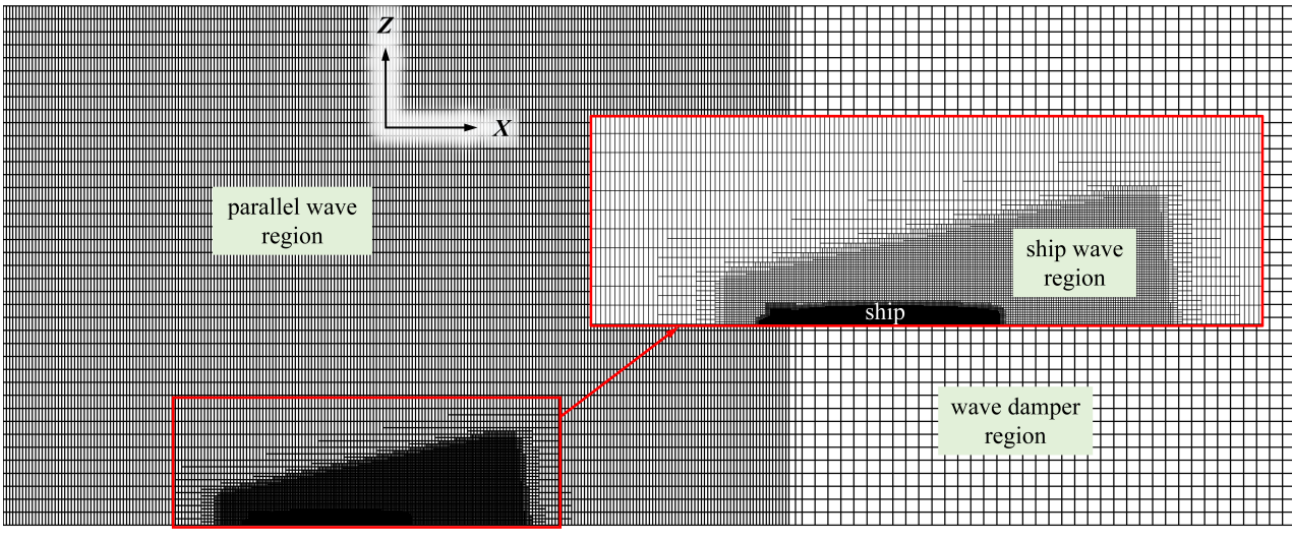

Figure 4. Top view of local successive refinement of the grid near the free surface.

Table 2. The refined mesh size of different regions.

Direction	Hull Surface Region	Hydrofoil Surface Region	Parallel Wave Region	Ship Wave Region
X	$\lambda/640$	$c/128$	$\lambda/80$	$\lambda/160$
Y	$\lambda/640$	$c/32$	$\lambda/20$	$\lambda/160$
Z	$\lambda/640$	$c/128$	$H/20$	$H/20$

3.3. Comparison and Validation

Although there are more and more researches on the hydrodynamic problems of bow foil wave-augmented propulsion system in recent years, there are still few recognized and systematic verifiable benchmark. In this section results are compared against other methods for the validation of the numerical scheme used for the hydrodynamic analysis of the examined system. The simulation in this paper involves ship wave, flapping foil, and wave problems, so the following three aspects are numerically verified separately.

3.3.1. Ship Wave and Resistance

Olivieri et al. [53] have carried out comprehensive towing tank experiments on the hydrodynamic characteristics of DTMB5415 model. In this paper, the results of calm water resistance and wave profiles in Olivieri are selected to verify the reliability of ISIS-CFD solver of FINE/Marine. Figure 5a shows the total resistance curves of dtmb5415 ship model as a function of carriage speed, and the wave profiles comparison at Fr = 0.28 are shown in Figure 5b. The CFD resistance curve is basically consistent with the measured results in experiments. The waveform of CFD results and experiment pictures are almost the identical in Figure 5b. The positions of the corresponding peaks and troughs are almost the same. In conclusion, the numerical method used in this paper is feasible and reliable for the resistance and ship wave analysis.

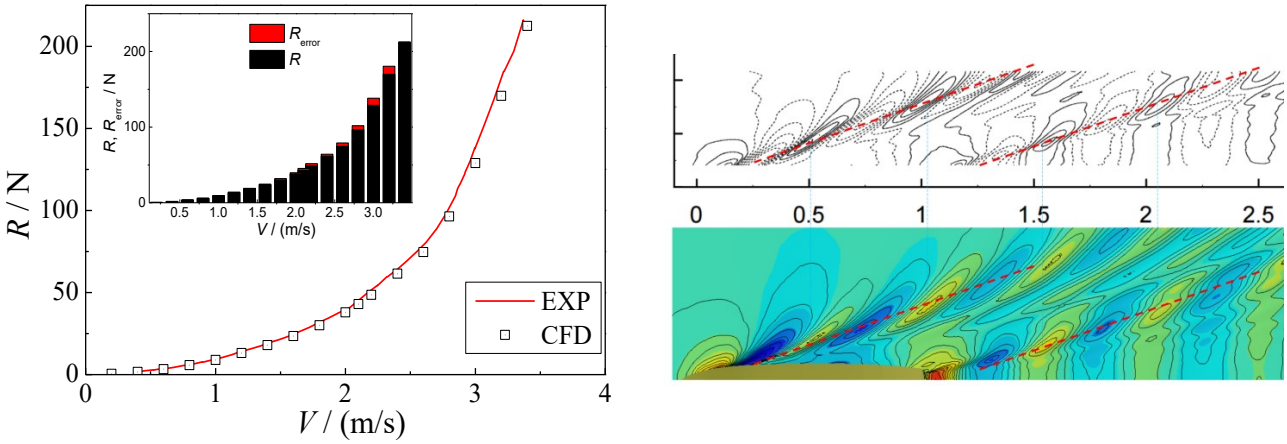

Figure 5. Comparison between DTMB5415 experimental results [53] and CFD results. (**a**) Resistance of DTMB5415 ship model. (**b**) Wave elevation contours of DTMB5415 ship model at Fr = 0.28.

3.3.2. Ship in Head Wave

In this part, the motion and force of DTMB5512 ship model, which are geometrically similar to DTMB5415, in the condition of head wave are simulated and compared with the experimental results of Irvine et al. [54] and Gui et al. [55]. The DTMB 5512 is a 3.048 m ship model (1/46.6 scale). The mesh and method adopted are similar to the settings in Section 3.2.

Eight working conditions are compared at different wavelengths under the conditions of Fr = 0.28, wave steepness $A{\cdot}K$ = 0.05 (where A is wave amplitude, K is wave number). In DTMB 5415 calculation conditions, $A{\cdot}K$ = 0.032, which is close to each other. The wave amplitude A and encounter frequency f_e at different wavelengths are shown in Table 3. The pitch radius of gyration for the hull is 0.25 Lpp, which follows the definition method of Formula 2 and Formula 3 in Irvine's work [54].

Table 3. Eight working conditions under the conditions of Fr = 0.28, wave steepness $A{\cdot}K$ = 0.05.

λ (m)	1.52	1.83	2.16	2.59	3.04	3.47	3.95	4.57
A (mm)	10.5	13.5	16.6	20.6	24.7	28	31.1	33.8
f_e (Hz)	2.02	1.763	1.561	1.369	1.22	1.112	1.017	0.918

First, the heave and pitch motion transfer functions TF_{x3} and TF_{x5} under different encounter frequencies f_e are compared, as shown in Figure 6. The detailed definitions of the two motion response parameters can be found in the literature [54]. From the comparison results, most of the calculated results are in good agreement with the experimental results except for individual working conditions under low frequency.

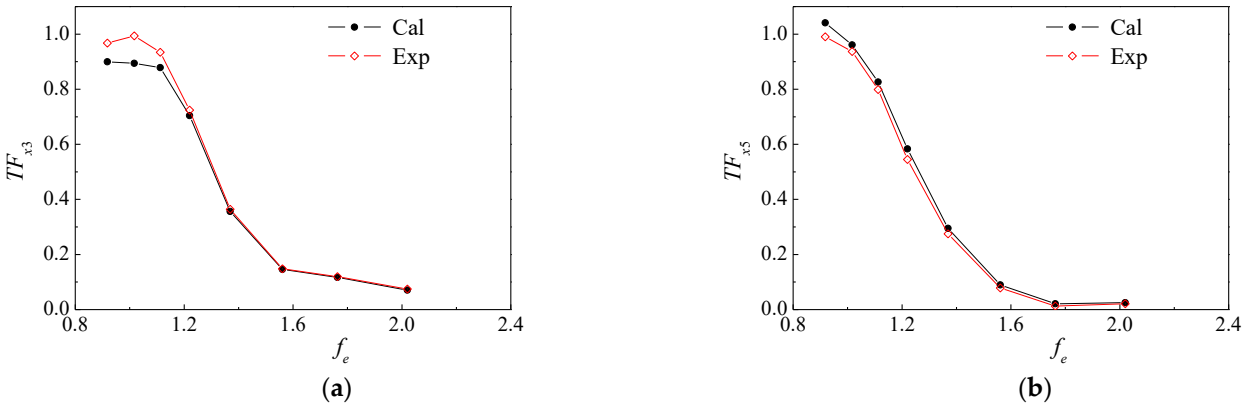

Figure 6. Comparison of numerical and experimental results of heave and pitch motion transfer functions TF_{x3} and TF_{x5} for different encounter frequencies f_e (**a**) TF_{x3}. (**b**) TF_{x5}.

Subsequently, the test results of force and moment on the hull for three wavelengths in the work of Gui [55] are compared with our simulation results. C_T, C_H, and C_M are resistance coefficient, heave force coefficient, and pitch moment coefficient, respectively. The definitions of these coefficients could be seen in literature [55] for details. The comparison results are shown in Figure 7. The overall trend of the comparison results of the three parameters is relatively consistent, with good coincidence at the minimum wavelength, followed by the maximum wavelength, and the worst coincidence at the middle wavelength. It is speculated that this is due to an increase in ship motion response with an increase in wavelength. At the same time, it is also considered that less data of the experiment may also affect the comparison, which needs further comparative research with the experiments in the future.

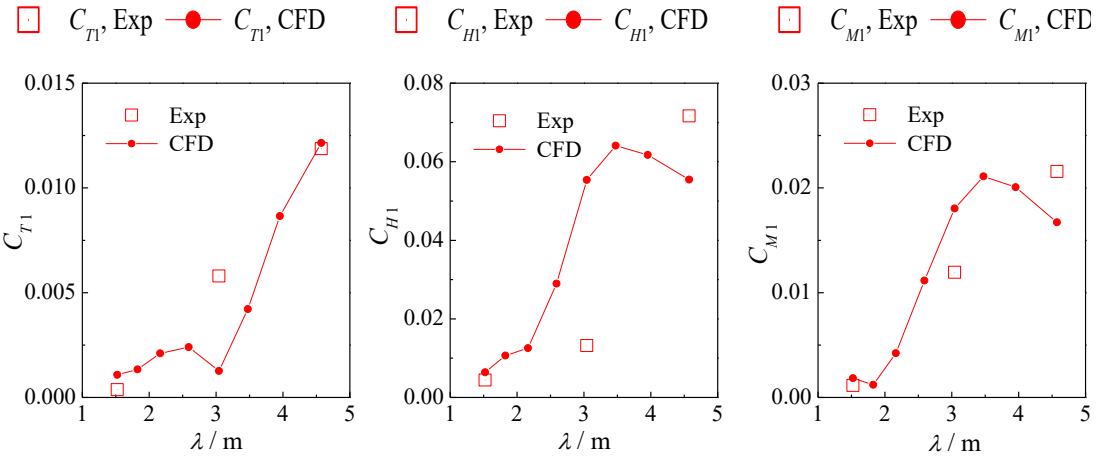

Figure 7. Numerical verification of hull force and moment coefficients at different wavelengths (the red box (□) is the test result of the literature and the red dot (.) is the CFD calculation result of this paper).

3.3.3. Flapping Foil Performance and Wake Vortex

In order to validate the numerical method used for flapping foil, selected benchmark conditions in Read's [42] and Schoveiler's [43] experiments are simulated, in which a rigid two-dimensional NACA 0012 airfoil is used. The heave amplitude-to-chord ratio is 0.75, the pitching axis is 1/3 chord from the leading edge of the airfoil, and maximum AoA $\alpha_{max} = 20°$. The comparisons of the efficiency η and thrust coefficients C_T for different S_t numbers are shown in Figure 8. The results in this paper are in good agreement with Read and Schoveiler's work. In addition, the calculation results under the same condition have

also been compared with data from those experiments results, as described by Schoveiler. Figure 9 is vorticity pattern visualized in the foil wake for St = 0.45, f = 1.2 Hz, a_{max} = 20°. The definitions of relevant parameters could refer to the expressions in the literature. The experimental and calculated results are compared and shown in Figure 9a,b separately, which agree with each other. In conclusion, the numerical method used in this paper is feasible and reliable for the hydrodynamic performance analysis of the flapping hydrofoil.

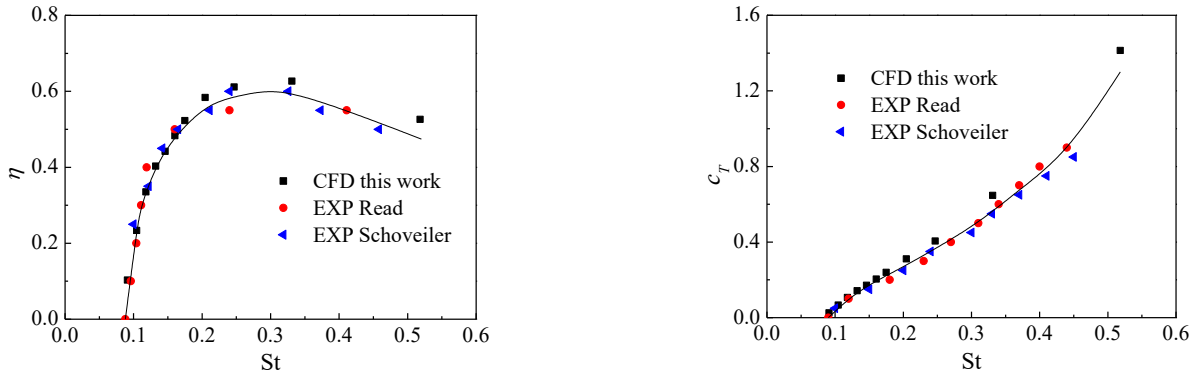

Figure 8. Comparisons of propulsive efficiency η and thrust coefficient c_T with previous computational and experimental results [42,43] (the black curve ■ is the CFD results of this paper; the red dot ● is the result of Read experiment; the blue triangle ▲ is the result of Schoveiler experiment). (**a**) Propulsive efficiency η. (**b**) Thrust coefficient c_T.

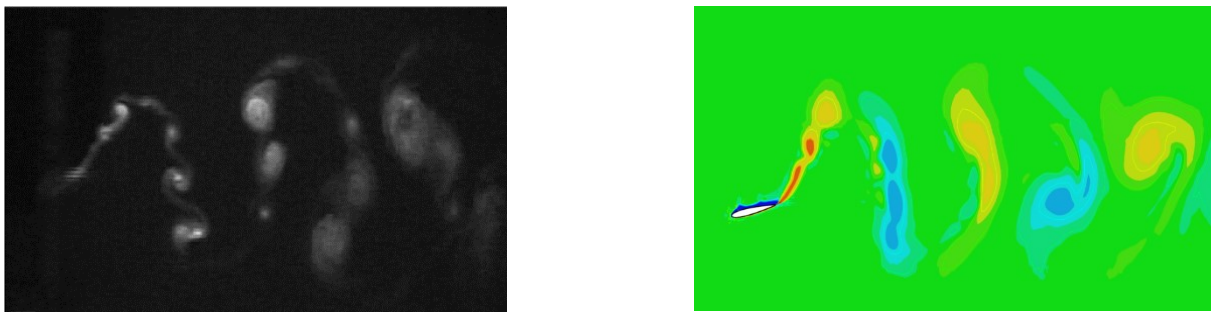

Figure 9. Vorticity pattern visualized in the foil wake for S_t = 0.45, α_{max} = 20°. (**a**) Experimental results of Schouveiler et al. 2005 [43]. (**b**) Numerical results in the current work.

4. Results and Analysis

In this section, the flow field, force, and motion of DTMB 5415 ship model with self-pitching bow foil in head waves under four speed conditions are simulated based on NUMECA software. First, the co-simulation of the ship with self-pitching bow foil in head waves is realized by ISIS-CFD solver, showing the complex interaction between the hull, bow foil, and waves, as well as the thrust-increase and drag-reduce effect of this wave-augmented propulsion system. Then, a series of studies are carried out for different torsion spring stiffness k and airfoil span h in different speed conditions. The effects of th two parameters on the drag reduction and thrust increase ability of the system are investigated individually by keeping all the other structural parameters constant with their baseline value, and the sensitivity of the performance to variation in several governing parameters is also evaluated in the current study. The Fr numbers corresponding to the four speeds under the conditions studied in this paper, spring stiffness, and span length of the bow foil are listed in Table 4.

Table 4. The parameters for the simulation.

Ship Model Speed V (m/s)	Froude Number ($\frac{V}{\sqrt{gL_{wl}}}$)	Torsion Spring Stiffness k (N × m/Rad)	Airfoil Span h (m)
0.5	0.067	4; 10; 20; 40; 60	0.4
1.0	0.134	10; 20; 40; 60; 80	0.4
1.5	0.200	20; 40; 60; 80; 100	0.4; 0.6; 0.8; 1.0
2.1	0.280	20; 40; 60; 80; 100	0.4

4.1. Co-Simulation Result

Figure 10 shows the simulation of the hull and self-pitching bow foil in head waves at four speeds, including total free-surface elevation of the ship model and the motion of the bow foil. The torsion spring stiffness adopted at each speed may also be observed in Figure 10. The time selected in each figure is the time when the bow foil reaches the maximum pitch angle under the corresponding working conditions. With the corresponding spring stiffness, the maximum pitch angle of the foil under the four working conditions is close. The pitch angle ranges from 6 to 7.5 degrees.

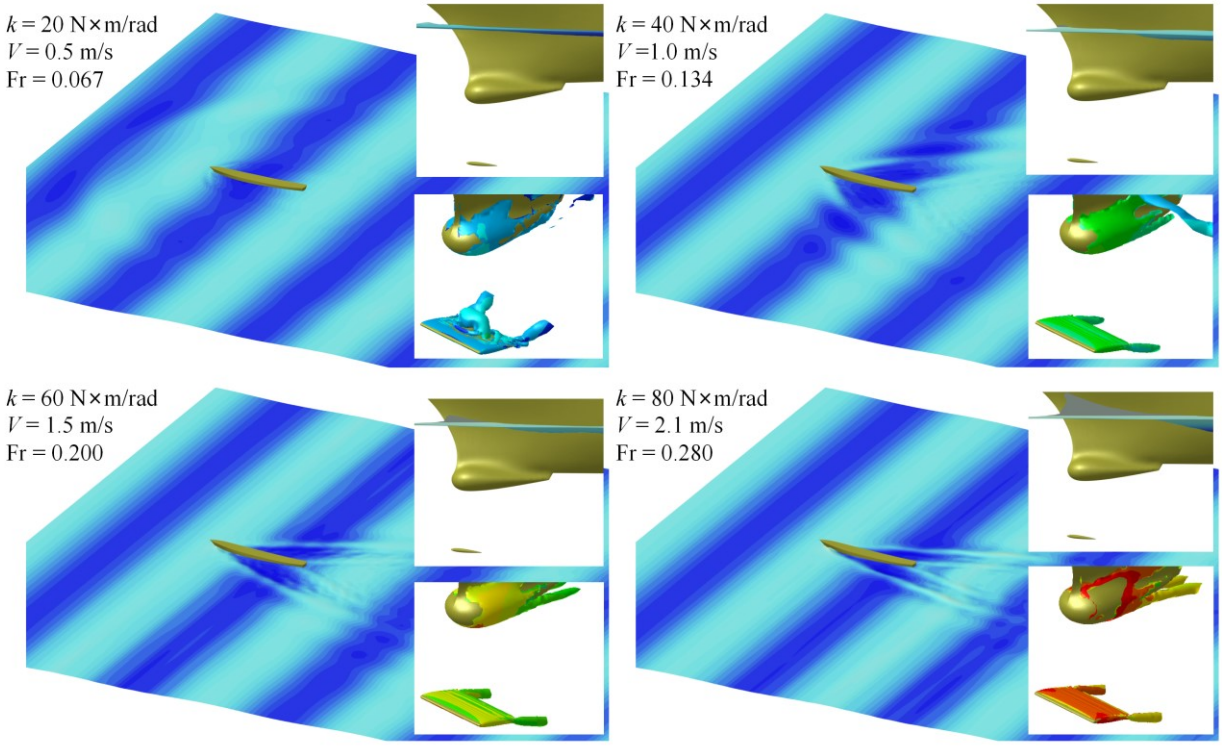

Figure 10. Simulation of the hull with self-pitching bow foil in head waves for different working conditions.

From Figure 10, it appears that the numerical method adopted in this paper can clearly exhibit the interaction between the hull and waves and realize simulation of self-pitching bow foil motion at the same time. The wake vortices of bow foil and the primary vortices of hull in the flow, namely sonar dome tip (SDTV) and windward bilge keel tip (BKTV) vortices [40], could be clearly distinguished in enlarged details in Figure 10. At higher speed, the wake vortex around the flapping foil shows typical tip vortex, which corresponds to the 3-D wake vortex characteristics at low St number. However, at lower speed (e.g., V = 0.5 m/s), the suction surface of the foil demonstrates an obvious separation vortex, which is consistent with the characteristics at high St number [56,57].

Since a small-amplitude wave is adopted in this paper, the pitching motion of the ship cannot be clearly distinguished in Figure 10. In order to clearly observe the motion of the hull and bow foil, the heave and pitch motion curves of the hull and bow foil in four working conditions are compared in Figures 11 and 12, respectively. The ordinates in the figures are all expressed as the magnitude of the parameter deviation from the equilibrium position.

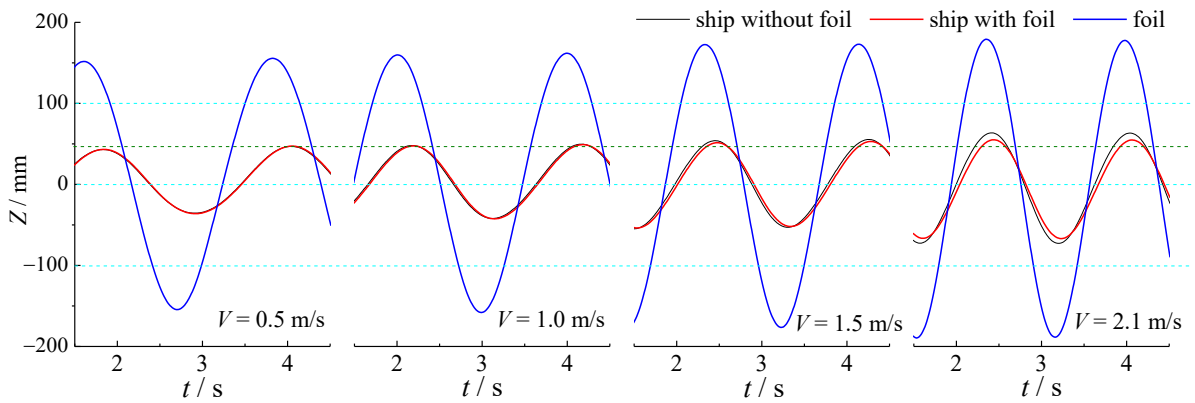

Figure 11. Heaving motion time–history curves of the hull and bow foil in head waves (black line: normal hull without bow foil; red line: hull with bow foil; blue line: rotation axis of bow foil).

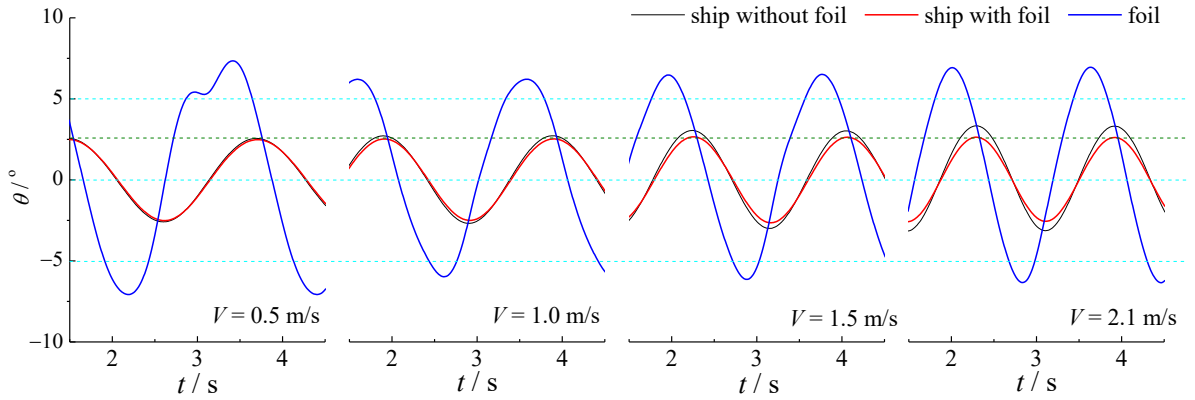

Figure 12. Pitching motion time–history curves of the hull and bow foil in head waves (black line: normal hull without bow foil; red line: hull with bow foil; blue line: rotation axis of bow foil).

First, from Figure 11, the heave amplitude of the bow foil (blue line) and the normal hull (black line) increase slightly with an increase in speed, but the heave amplitude of the bow foil is obviously larger than that of the hull. For the working condition in this paper, the heave amplitude of the bow foil is about three times the wave amplitude. This is because the heave motion of the bow foil is affected by the combined action of the heave and pitch motion of the hull, and the heave amplitude of the flapping foil is closely related to the amount of energy/power it absorbs, so this is a very favorable phenomenon for wave-augmented propulsion technology and also suggests that we should design the parameters of the bow foil according to the sea condition instead of hull motion in engineering applications. Second, it can be seen from Figure 11 that, at higher speeds (V = 2.1 m/s), the heave amplitude of the hull with bow foil (red line) is slightly lower than that of the normal hull (black line), but this phenomenon is not obvious at lower speeds. This is because, with an increase in speed, when the heave amplitude of the bow foil increases obviously, the characteristic speed of its heave motion increases, which leads to an increase in hydrodynamic force, and then the input power (i.e., the absorbed power)

increases. That is, for the hull, the bow foil is equivalent to damping. At higher speeds, due to the damping effect of bow foil, the heave amplitude of the hull with foil is slightly lower than that of normal hulls. It makes the heave amplitude of the hull with foil change very little at different speeds; that is, the bow foil plays a good damping role on the hull heave motion.

A comparison of the pitching motion of the normal hull, the hull with bow foil, and the bow foil is shown in Figure 12. On one hand, similar to the heave motion in Figure 11, at higher speeds, the pitch amplitude of the normal hull gradually increases (black line). The pitch amplitude of the hull with bow foil (red line) is lower than that of the normal hull (black line), and this phenomenon is obvious at higher speeds. That is, the damping effect of the bow foil is more obvious to the pitching motion of the hull and even exceeds the influence of heave motion [16,25]. On the other hand, pitch amplitude of the hull with bow foil (red line) does not change significantly with an increase in speed and remains basically unchanged because of the damping effect of bow foil. At the same time, the pitching amplitude of the bow foil (blue line) neither changes significantly with an increase in speed and remains basically unchanged. This is because the semi-active elastic flapping foil is a complex spring-mass system. Its heave motion is directly generated by the motion of the ship, while the pitch motion parameters are affected by the combined action of hydrodynamic moment and torsion spring [47]. At the same time, unlike the single semi-active elastic flapping foil, the pitch motion of bow foil also involves interaction with the wave surface and the hull, and the mechanism is more complex. It requires further systematic study. In conclusion, additional bow foil devices contribute to decreasing heave and pitch motions. This fact has been repeatedly noted in the literature [17,20,58].

From the above results, as speed increases, the damping effect of the bow foil becomes larger, and the influence of bow foil on the motion of the hull becomes larger, which further affects the force on the hull. In order to further analyze, Figure 13 shows the hydrodynamic force in X direction (F_x) of the hull and bow foil under different working conditions. Since the ship is sailing in the negative direction of the x-axis, the resistance of hull is positive on average. On the contrary, the additional thrust generated by the foil is negative. It can be clearly seen from Figure 13 that the resistance of hull with bow foil (red line) is smaller to that of ordinary hull (black line). At the same time, this trend is more obvious with an increase in speed. At a higher speed (V = 2.1 m/s), due to the increased influence of the bow foil, the time–history curve of ship resistance has changed significantly. The bow foil added not only reduces the resistance of the ship but also smooths the high-order resistance at high speed. However, at a lower speed (V = 0.5 m/s), the bow foil has little effect on hull resistance.

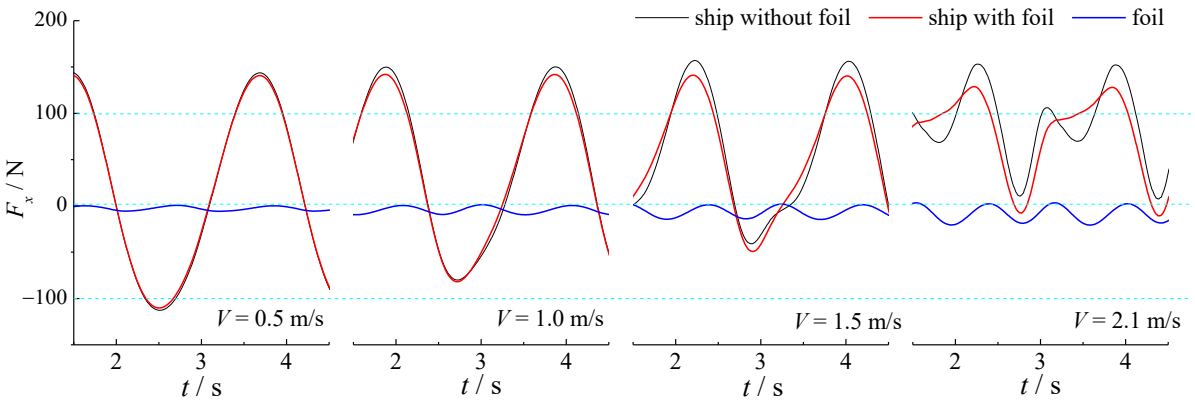

Figure 13. Time traces of the axial force F_x acting on the hull and flapping foil (black line: normal hull without bow foil; red line: hull with bow foil; blue line:rotation axis of bow foil).

In order to quantitatively analyze the effect of thrust increase and drag reduction of the bow foil wave-augmented propulsion system, the time average of the hull resistance

and thrust of the foil under the above four working conditions was carried out for the whole period, and the comparative analysis was carried out with the calm water resistance and resistance in waves of ordinary hull. The relationship between the components is shown in Figure 14. The working conditions and definitions of various hydrodynamic parameters are shown in Table 5. On the whole, with an increase in speed, the four hydrodynamic parameters increase with an increase in speed, but the increasing speed is slightly different. The resistance of the hull with bow foil (R_{WF}) is significantly lower than that of the conventional hull under the same working condition. When the speed is 2.1 m/s, the difference between the two resistances is about 10N, and the decreased resistance of the hull reaches about 11%. It is speculated that this is due to the damping effect of the bow foil on the ship's motion, which has been discussed in Figures 11 and 12. This damping could weaken the ship's motion in the waves so that the ship's resistance is slightly reduced. At the same time, with an increase in speed, the thrust of the bow foil (T_F) increases gradually, but the growth rate is less than the calm water resistance of the normal hull. If the reduced resistance of the hull and the increased thrust of the bow foil are considered at the same time, the drag reduction effect of the ship with bow foil wave-augmented propulsion system is more obvious.

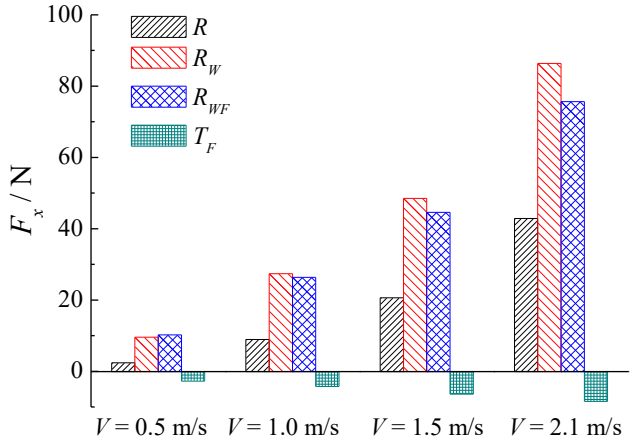

Figure 14. Mean axial force F_x acting on the hull and bow foil.

Table 5. The hydrodynamic force defined in Figure 13.

Hydrodynamic Force (N)	Working Condition	Ship Type	Definition
R	calm water	Ship without foil	axial force acting on hull in calm water
R_W	in head wave	Ship without foil	axial force acting on hull in waves
R_{WF}	in head wave	Ship with bow foil	axial force acting on hull in waves
T_F	in head wave	Ship with bow foil	axial force acting on bow foil in waves

The principal mechanism of the bow foil was found to be two-fold [47]: increased thrust generated by the bow foil and reduced added resistance in waves by damping effect of the bow foil. The design of the foil will affect the ratio of these two mechanisms, and it is, therefore, important to understand the contribution of each part. Assuming small deviations in propulsive coefficient in waves, resistance in calm water of the hull can approximately represent the thrust of the ship propeller. Using the measured foil thrust, the estimated percentage contributions due to foil thrust and thrust enhancement ratio (r_{TE}) are defined as Equation (9) and shown in Figure 15.

$$r_{TE} = \frac{T_F}{R} \tag{9}$$

The resistance reduction ratio of the bow foil is defined as the reduction ratio of the total resistance of the ship with bow foil compared with the resistance of the bare hull in waves. The total resistance of a ship with bow foil is expressed as the sum of the hull resistance R_{WF} and the bow foil thrust T_F. The resistance reduction ratio in head waves is expressed as:

$$r_R = \frac{R_W - (R_{WF} + T_F)}{R_W} \tag{10}$$

In the four working conditions in Figure 10, the thrust enhancement ratio (r_{TE}) of the bow foil wave-augmented propulsion system is about 20–115%, which is consistent with the conclusion achieved by Bowker [24], and the resistance reduction ratio r_R is about 19–27%. However, this is not an exact method and has only been used to provide an estimate of the relative effect of a change in added resistance compared to the additional thrust provided by the bow foil. However, it is certain that the thrust increase and drag reduction effect of the bow foil is noticeable. This represents significant energy saving in head seas with use of the bow foil.

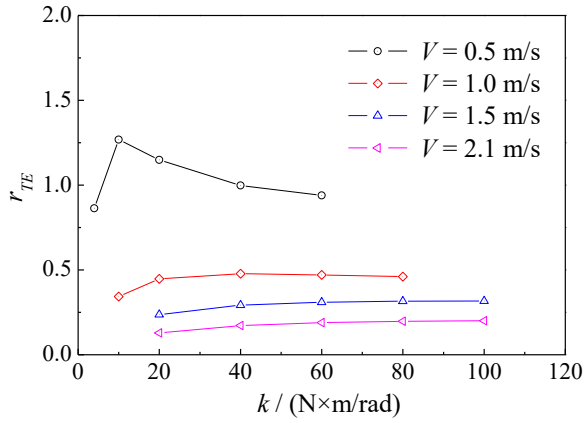

Figure 15. Thrust enhancement ratio (r_{TE}) of bow foil at different speeds and different spring stiffness.

4.2. Effect of Torsion Spring Stiffness

The bow foil adopted in this paper is semi-active flapping foil with a spring-mass system. According to research on semi-active flapping foil [44], the performance of this kind of flapping foil is closely related to St number and spring stiffness, so we first analyzed the thrust increase and drag decrease effects of the bow foil wave-augmented propulsion system under different spring stiffness.

Figure 15 shows the thrust enhancement ratio (r_{TE}) of bow foil with different spring stiffness (k) at four speeds. On the whole, at the same speed, the spring stiffness has less influence on thrust enhancement ratio. Compared with the spring stiffness, the ship speed has more obvious influence on the thrust enhancement ratio. The thrust enhancement ratio is greater at lower speed. At the speed of V = 0.5 m/s, the thrust enhancement ratio can reach as high as 125%. However, with an increase in ship speed, the increased speed of the bow foil thrust is slower than that of the hydrostatic resistance, so, at the higher speed (V = 2.1 m/s), thrust enhancement ratio is reduced to about 20%. In addition, it can be seen from the thrust enhancement ratio results of three higher speeds (three solid lines in red, blue, and pink in Figure 15) that, with an increase in spring stiffness ratio, the thrust enhancement ratio gradually increases and then tends to a stable value. Different from the case of high speed, at low speed (black line in Figure 15), the spring stiffness has a greater impact on the thrust enhancement ratio. With an increase in the spring stiffness ratio, the

thrust enhancement ratio first increases and then decreases, reaching the extreme value when the spring stiffness k = 10 N × m/rad.

Figure 16 further compares the resistance reduction ratio r_R of bow foil with different spring stiffness at four speeds. According to the definition of resistance reduction ratio (Equation (9)), the reduction ratio determines the overall energy-saving effect of the bow foil system on the hull. As a whole, the spring stiffness has different effects on the reduction ratio of the bow foil at different speeds. Similar to the influence of thrust enhancement ratio in Figure 15, spring stiffness has a greater influence on resistance reduction ratio at low speed (V = 0.5 m/s). When the spring stiffness k = 10 N × m/rad, the resistance reduction ratio reaches 27%. At the other three higher speeds, the spring stiffness has less influence on the resistance reduction ratio, which is roughly stable at about 20%. At the same time, it can be roughly observed that, with an increase in speed, high spring stiffness has a positive impact on increase in resistance reduction ratio. Considering the adaptability to different speed requirements, it is more appropriate to select k = 35 N × m/rad in this paper, which can achieve a resistance reduction ratio of more than 15% at each speed. Furthermore, to sum up the analysis of the above two parts, it is necessary to optimize the spring stiffness in the design of a semi-passive flapping foil wave-augmented propulsion system.

$$k\prime = \frac{k}{\rho(f_e B_0)^2 hc^2} \tag{11}$$

$$KT = \frac{T_F}{\rho(f_e B_0)^2 hc} \tag{12}$$

The above only roughly observed the effect of thrust increase and drag reduction of the flapping foil, but it is difficult to explain the hydrodynamic characteristic of bow foil with different spring stiffness. This is because the Strouhal number ($S_t = f_e B_0 / V$, where B_0 is average sweep width of flapping foil (m)), has been shown to be an important metric for the propulsive efficiency of flapping foil propulsion [44]. In order to consider the influence of St number and spring stiffness comprehensively, we first analyzed the St number of the bow foil used in this paper, and the results are shown in Figure 17. Then, referring to the work of Thaweewat et al., the spring stiffness and the thrust of the flapping foil were unified dimensionless, and the spring stiffness coefficient k' and thrust coefficient KT were expressed as Formulas (11) and (12), respectively. In Figure 18, the change in thrust coefficient KT with St number and spring stiffness coefficient k' is further shown.

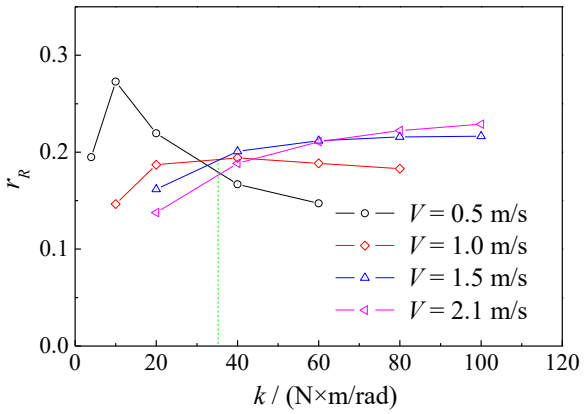

Figure 16. Resistance reduction ratio r_R of bow foil with different speeds and different spring stiffness.

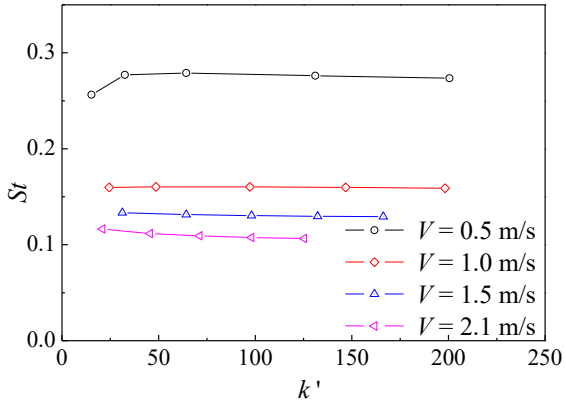

Figure 17. St number of bow foil at different speeds and different spring stiffness in this paper.

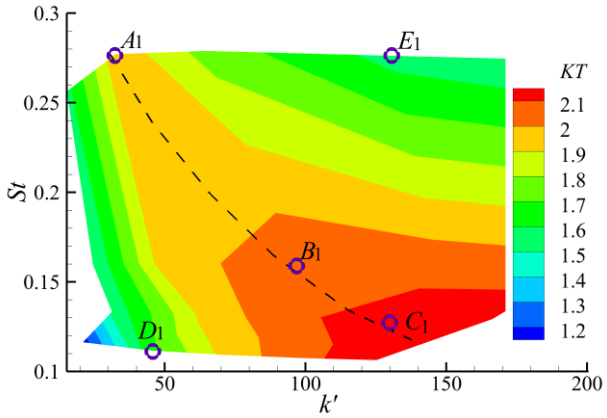

Figure 18. Thrust coefficient distribution diagram of bow foil with different S_t numbers and different spring stiffness.

It can be seen from Figure 17 that the S_t number of the ship bow flapping foil at different speeds changes little with the spring stiffness coefficient, which is mainly determined by the speed. This is because, at a certain speed, the encounter frequency of the ship relative to the waves is constant. At the same time, it can be seen from the heaving motion curve of the swinging wing in Figure 11 that, when the spring stiffness is changed, the heaving amplitude of the bow foil is also less affected, that is, the sweep width of the bow foil is relatively stable in regular waves. Therefore, according to the definition of St number, its change with spring stiffness coefficient is small. The St number of the semi-active bow foil in this paper is about 0.27 at low speed (V = 0.5 m/s), close to the optimum values of between 0.25 and 0.35 for propulsive efficiency [59]. At higher speed, the St number of the semi-active bow foil is between 0.1–0.16, which is close to the mean Strouhal number of 0.13 in Bowker's work [25]. Whilst this is an interesting observation, the parameters that govern the St number for bow foil wave propulsion are dictated by ship speed, scale, and environment, all of which are predetermined.

In Figure 18, the distribution of KT shows an obvious ridge shape. The overall trend is that, when the bow foil works at a small St number (i.e., at a higher speed), the corresponding maximum thrust coefficient appears at the position with a larger spring stiffness coefficient. On the contrary, when the bow foil works at a large St number (i.e., at a lower speed), the corresponding maximum thrust coefficient changes to a position with a smaller spring stiffness coefficient. That is, a smaller St number and a larger spring stiffness coefficient are in favor of achieving a larger thrust coefficient of bow foil, which is consistent with our previous results of the semi-active flapping foil propulsion performance [45]. At the same time, this conclusion is also consistent with the results in Figure 14; that is, under

the conditions of V = 2.1 m/s and k = 100 N × m/rad, the thrust of the bow foil increases significantly. To sum up, there is a dilemma in the selection of the spring stiffness ratio. For a bow foil, the spring stiffness and moment of inertia are determined when the design has been finalized. When the pitching frequency and amplitude are constant, it is difficult to work efficiently at a higher St if a smaller spring stiffness ratio k' is used to achieve a higher thrust in the low St state. On the contrary, if a larger k' is used to achieve high thrust and high efficiency at lower St, the thrust at starting state will be small. However, a design idea can be provided here. Different spring stiffness ratios can be obtained by changing the airfoil span h in order to achieve high performance in various working states. According to this analysis, semi-active bow foil can be designed to have a relatively high spring stiffness ratio. When more thrust is required, for example, in the starting state, the spring stiffness ratio can be reduced by increasing the airfoil span h so as to obtain more thrust.

According to the force on the airfoil and the working state of the bow foil, the thrust generated is closely related to the pitch angle θ and AoA α. The spring stiffness of the flapping foil and the sailing speed of the ship model will affect the pitch angle and AoA, so it is difficult to clearly explain the change mechanism of its thrust under different working conditions. Figure 19 shows the time–history of pitch angle θ and AoA α under five working conditions. The corresponding positions of the five working conditions are marked in Figure 18, including three points distributed on the KT ridge line and two points with smaller KT.

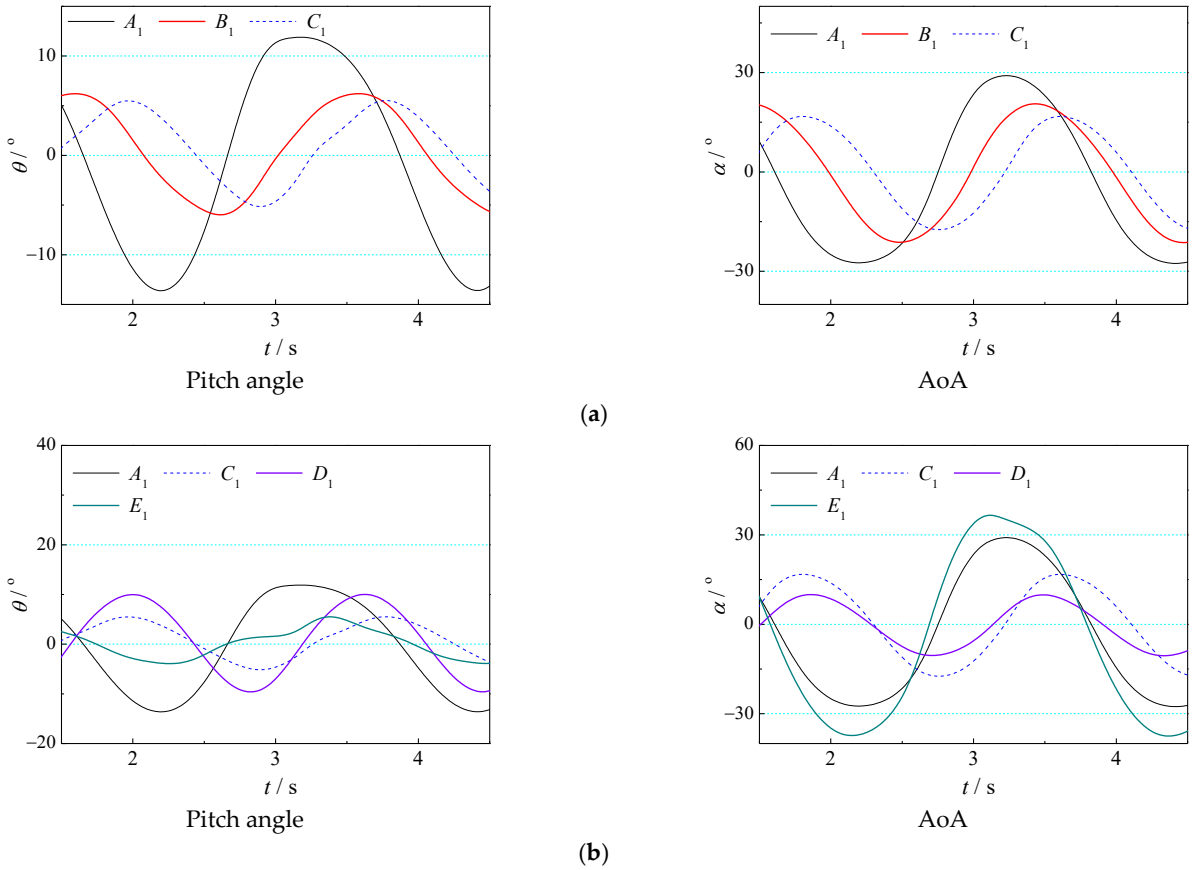

Figure 19. The time–history of pitch angle θ and AoA α under five working conditions in Figure 18. (**a**) Time traces of the pitch angle and AoA of three working points A_1, B_1, and C_1. (**b**) Time traces of the pitch angle and AoA of four working points A_1, E_1, C_1, and D_1.

The pitch angle θ and AoA α of three working points A_1, B_1, and C_1, which have high thrust coefficients, are compared in Figure 19a. As a whole, the time–history of the pitch angle and AoA of these three points are close to the sine curve, and the pitch motion period

of the three working conditions increases with a decrease in St (increase in speed). Because the spring stiffness coefficients are well matched with St in these three working points, the pitch angles are all controlled at about 5–12°, and the maximum AoA is concentrated between 15° and 30°. With an increase in the spring stiffness from point A_1 to point C_1, the pitch angle gradually decreases, and the maximum AoA gradually approaches the optimal AoA of the semi-active flapping foil (15°) [44]. Therefore, the thrust coefficient from point A to point C also increases gradually.

Figure 19b further compares four working points A_1, E_1, C_1, and D_1. Both points A_1 and E_1 have approximately higher St numbers but different spring stiffness coefficients. Points A_1 and D_1 have similar lower spring stiffness coefficients, but the St numbers are different. As a whole, the maximum pitch angle of each point is small, which is roughly distributed in the range of 5–12°, while the range of maximum AoA α is much larger, which is roughly distributed in the range of 10–35°. Specifically, the pitch amplitude of point A_1 and point D_1 with smaller spring stiffness ratios is larger, both above 10°. The pitch amplitude of C_1 and E_1 is small, which corresponds to the spring stiffness ratio of both being large. It can be roughly understood that, when the spring stiffness coefficient is low, the ability of the flapping foil to resist hydrodynamic action is poor, so the pitch angle amplitude is large, that is, the pitch angle is more sensitive to the change in the spring stiffness coefficient. However, under different St, the AoA of the flapping foil is affected by the pitch angle and advance speed at the same time, so the AoA of the four points differ greatly. The AoA at point A_1 is as high as 30°, while that at point D_1 is only about 10°. The AoA at point C_1 is 15°, and that at point E_1 is as high as 35°. At the same St number as C_1 and D_1, when the spring stiffness coefficient is high, the ability of the flapping foil to resist hydrodynamic action is strong, so the AoA at point C_1 is larger than that at point D_1. However, by comparing the thrust coefficients of these points, it is found that too large and too small AoA are not conducive to generation of thrust (such as point D_1 and point E_1). Here, it is speculated that the thrust of semi-active flapping foil has a similar dependence on the AoA to that of efficiency (Thaweewat et al., 2018), but a large number of results are needed to further verify this opinion. In addition, it is found that the asymmetry of the pitch motion track is aggravated in condition A_1 and E_1. This finding is likely to be due to a contribution of both the phase response relative to the oscillating flow of the incident wave profile [25] and the large separation caused by the excessive AoA. The wake vortex diagrams of the A_1 and E_1 working conditions are shown in Figure 20. At the moment when the pitch angle is 0 and the AoA is maximum, large separation occurs on the bow foil surface under both A_1 and E_1 conditions. Moreover, due to the larger AoA under E_1 working condition, the surface separation is more intense, which is consistent with the speculation. The similar phenomenon of asymmetric trajectory has been found in the research of double elastic flapping foil [47] but still needs to be further studied in the semi-active bow foil wave-augmented system.

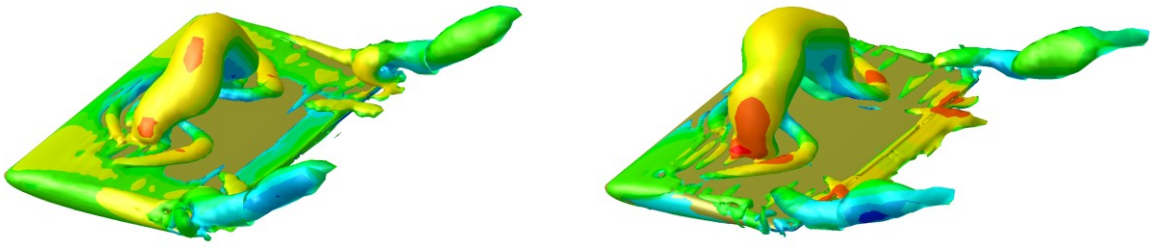

Figure 20. Wake vortex diagrams of working conditions A1 and E1 at the moment of $\theta = 0$.

4.3. Damping Effect of the Bow Foil Span

In the discussion in Section 4.1, it is found that the preliminarily designed bow foil in this paper has little effect on the hull at low speed; that is, it does not fully absorb wave

energy, and, at the same time, it cannot well explain the relationship between suppression of hull motion response and hull drag reduction. Therefore, this part will adjust the span of the bow foil in order to increase the hydrodynamic force of the bow foil, thereby enhancing the coupling relationship between the flapping foil, hull, and waves and exploring the interaction between them.

In this part, the ship speed V = 1.5 m/s (Fr = 2.0) is selected for analysis; the selected foil spans are h = 0.4 m, 0.6 m, 0.8 m, and 1 m, respectively. Among them, h = 0.8 m is slightly larger than the ship width, while h = 1 m is obviously larger than the ship width. The corresponding aspect ratio of foil is h/c = 2, 3, 4, and 5, respectively.

The thrust enhancement ratio and resistance reduction ratio of the bow foil to the hull under different spring stiffness coefficients and span lengths are shown in Figure 21. With an increase in foil span, both the thrust enhancement ratio and resistance reduction ratio of the bow foil are significantly improved, but the increase rate is gradually reduced. This is because, with an increase in the span length of the bow foil, its hydrodynamic force increases, which further inhibits the movement of the ship in waves, thus reducing the heave amplitude of the bow foil. Therefore, the increasing amplitude of the hydrodynamic effect of the bow foil, which increases with the span, becomes weaker. In addition, it can be further determined from Figure 21 that, with an increase in spring stiffness ratio, the thrust enhancement ratio and resistance reduction ratio of the bow foil also increase gradually and the increase amplitude becomes lower and lower and finally tends to a fixed value. This is mainly because, under higher spring stiffness, the swing angle of the swing wing is small, so the change in spring stiffness has little effect on it, and, furthermore, the change in its AoA is small, so its thrust performance becomes insensitive to spring stiffness. This is because, under higher spring stiffness, the pitch angle of the bow foil is small, so the change in spring stiffness has little influence on pitch angle, and, furthermore, a change in spring stiffness will have little influence on the change in AoA. Therefore, the bow foil thrust performance becomes insensitive to spring stiffness at higher spring stiffness.

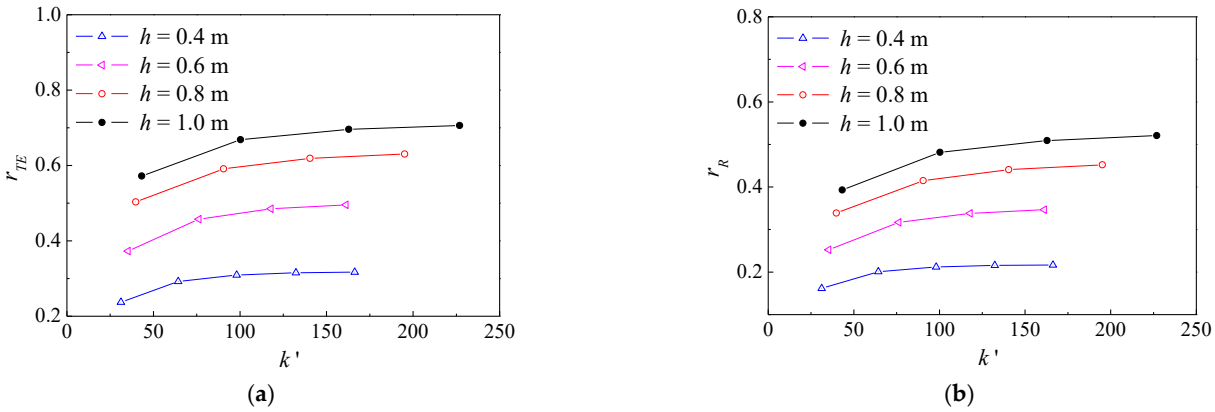

Figure 21. The change in thrust enhancement ratio and resistance reduction ratio of bow foil with different spring stiffness and different spans. (**a**) Thrust enhancement ratio r_{TE}. (**b**) Resistance reduction ratio r_R.

In the range of foil span and spring stiffness discussed in this section, the thrust enhancement ratio is roughly in the range of 24–71%, while the resistance reduction ratio is roughly in the range of 16–52%. This is an exciting result for energy conservation and emission reduction of the hull. Perhaps further increasing the foil span could still increase the thrust enhancement ratio and resistance reduction ratio of the system, but it lacks practical significance to discuss the limit thrust increase rate and drag reduction rate only under the wave conditions set in this paper. This is because, on the one hand, excessive hydrofoil span has certain hidden dangers in the structure, such as collision or fracture; on the other hand, the thrust increase and drag reduction ability of the bow foil system are

also closely related to the actual sea conditions, so it is more practical to analyze them in combination with the sea conditions, which is also our next work to be carried out.

In order to analyze the coupling effect between the bow foil and the hull, Figure 22 shows the cloud diagram of the heaving motion amplitude at the bow position (actually the bow foil shaft position) under different spring stiffness and hydrofoil span. The heaving motion amplitude of the ship bow B_0 decreases significantly with an increase in hydrofoil span and spring stiffness. Figure 23 also shows the average resistance of the hull R_{wF} and the average thrust of the bow foil T_F under different hydrofoil spans and different spring stiffness. By comparing Figures 22 and 23, the effect of the bow foil system on the hull in waves could be reflected in two aspects: on the one hand, the additional thrust provided by the bow foil, and, on the other hand, the resistance in waves of the hull is reduced due to suppression of the bow foil on hull movement.

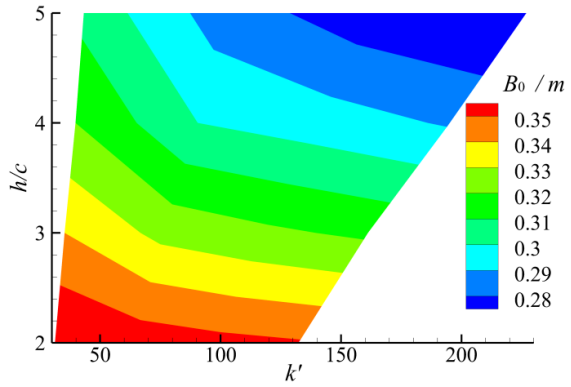

Figure 22. Distribution diagram of ship bow heaving amplitude under different span and spring stiffness.

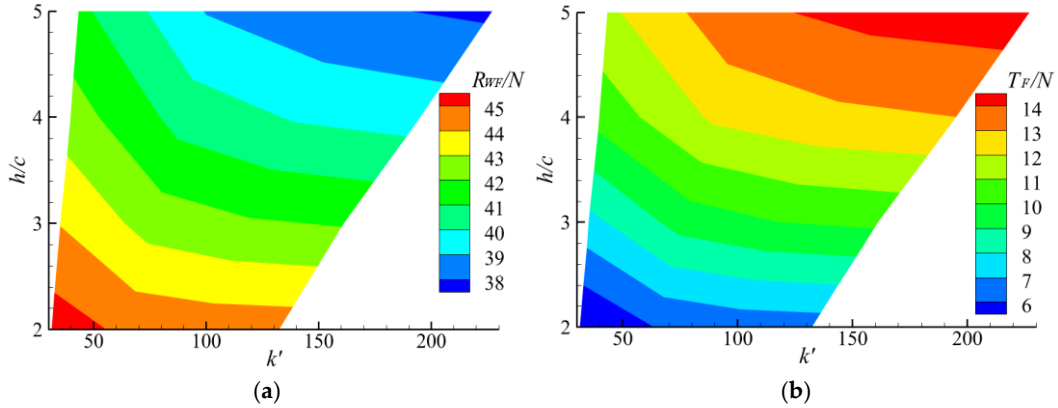

Figure 23. Distribution diagram of hull resistance R_{WF} and flapping foil thrust T_F under different span and spring stiffness. (**a**) Hull resistance R_{WF}. (**b**) Flapping foil thrust T_F.

Finally, the influence of different thrust-increasing effects of the bow foil system on wave surface was observed. Two points with the lowest and highest thrust-increasing effects under V = 1.5 m/s working condition were selected, namely with the minimum spring stiffness and h = 0.4 m condition and the maximum spring stiffness and h = 1.0 m condition. The wave surface cloud diagrams of these two working conditions are shown in Figure 24. On the whole, the ship wave in Figure 24b is slightly weaker than that in Figure 24a. The head wave crest on the left side is higher and its wake is more obvious. In contrast, the stern wave on the right side is more discrete, the wave crest is not obvious enough, and the head wave is also more discrete. This corresponds to the hull resistance analyzed above. The right-side condition has less energy dissipation and hull resistance due to weak ship waves. In order to observe the ship wave more clearly, the distribution of

wave height along the Y coordinate axis was observed at different distances from the stern. The X coordinate axis of the observation position was 7 m, 8 m, 9 m, and 10 m, respectively, as shown in Figure 24. Since ship waves are almost symmetrical, only the wave height curve on one side is shown in Figure 25. It can be clearly seen from the figure that, under the working conditions of $h = 1.0$ m $k = 200$ N $\times$ m/rad, the wave height of the ship wave is generally smaller than that under the other working condition, which also shows that the bow foil can inhibit ship motion.

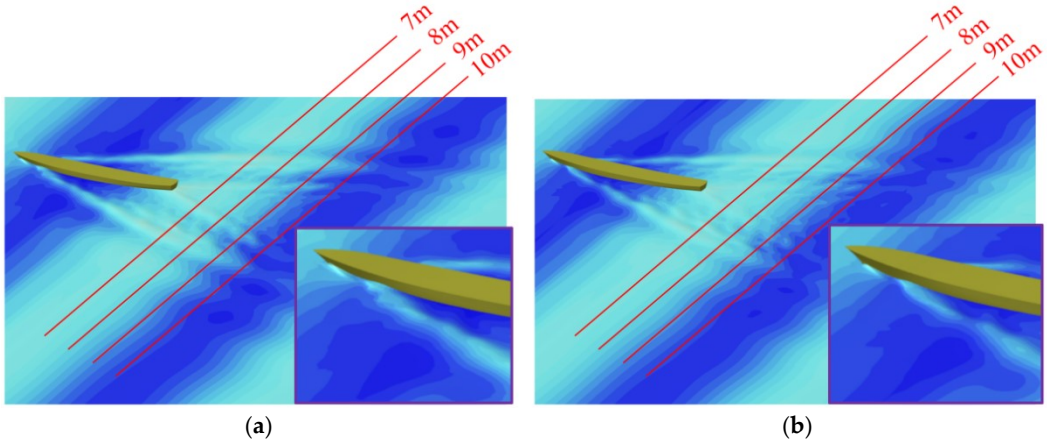

Figure 24. Free-surface elevation of the hull under the action of bow foil with different span lengths and different spring stiffness. (**a**) $h = 0.4$ m $k = 20$ N $\times$ m/rad. (**b**) $h = 1.0$ m $k = 200$ N $\times$ m/rad.

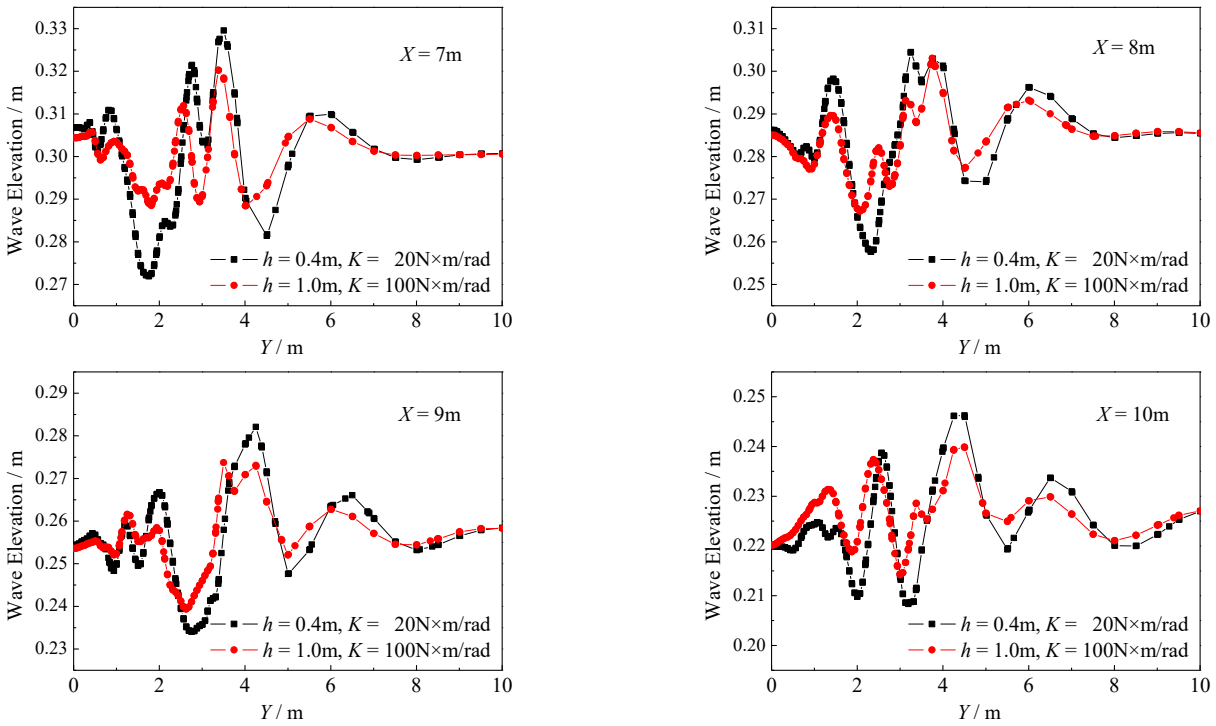

Figure 25. Distribution of wave heights along Y coordinate at four X coordinate positions in Figure 24.

5. Conclusions

The drag reduction mechanism of elastic bow foil on ship hull in waves is discussed in this paper. It can be observed preliminarily that the effect of the bow foil on the hull in waves is reflected twofold: on the one hand, the additional thrust provided by the bow foil;

on the other hand, the damping effect of the bow foil on the hull, which reduces the motion response of the hull in waves and also reduces added resistance in waves.

- In this paper, the ISIS-CFD solver based on NUMECA software is used to realize joint simulation of a ship with semi-active elastic flapping foil in head waves. The complex interaction between the hull, flapping foil, and waves is considered, which enriches the analysis methods of such problems;
- In numerical simulation, the increasing thrust and reducing drag effect of the elastic flapping foil to the ship in waves is preliminarily realized. In the range of bow foil span and spring stiffness discussed in this paper, the thrust enhancement ratio is roughly in the range of 24–71%, while the drag reduction rate is roughly in the range of 16–52%. Under the working condition of $V = 1.5\mathrm{m/s}$ (Fr = 2.0), the resistance reduction ratio exceeds 50%, which represents significant energy saving in head seas with use of the bow foil.
- This paper discusses the influence of key design parameters on the thrust-increasing and drag reducing capability of a semi-active bow foil system, including spring stiffness and flapping foil span. It can be roughly determined that there can be an optimal range of spring stiffness so that the hull with bow foil system can have the effect of increasing thrust and reducing drag in a large range of speed. The longer the span of the flapping foil is, the better the effect of thrust increase and drag reduction to the hull is. However, the thrust increase ratio and drag reduction rate of the system become more and more gentle with an increase in span length.

In the future, on the one hand, the bow foil thrust enhancement mechanism should be further expanded, including the influence of flapping foil phase difference, encounter frequency, and foil submergence depth on the drag reduction and thrust enhancement effect. On the other hand, it can form a bow foil incremental effect prediction model, which can be further extended to estimate emissions of CO_2 from ships, which will be a more direct evaluation of how this green ship technology can help with marine environment protection.

Author Contributions: Conceptualization, J.Z. and L.M.; methodology, W.Y. and J.Z.; investigation, J.Z. and L.M.; validation, W.Y.; writing—original draft preparation, J.Z. and L.M.; writing—review and editing, L.M., W.S. and W.Y. All authors have read and agreed to the published version of the manuscript.

Funding: This research was funded by the Advanced Aviation Power Innovation Workstation project (grant no. HKCX-2019-01-005 and HKCX2020-02-024) and the Shandong Province Science and Technology Development Plan Item (grant no. 2013GGA10065).

Institutional Review Board Statement: Not applicable.

Informed Consent Statement: Not applicable.

Data Availability Statement: Data is unavailable due to privacy or ethical restrictions.

Conflicts of Interest: The authors declare no conflict of interest.

References

1. Hu, L.; Wu, H.; Yuan, Z.; Li, W.; Wang, X. Roll motion response analysis of damaged ships in beam waves. *Ocean Eng.* **2021**, *2*, 108558. [CrossRef]
2. Belibassakis, K.; Bleuanus, S.; Vermeiden, J.; Townsend, N. Combined performance of innovative biomimetic ship propulsion system in waves with Dual Fuel ship engine and application to short-sea shipping. In Proceedings of the 31st International Ocean and Polar Engineering Conference, Rhodes, Greece, 20–25 June 2021.
3. Lee, J.H.; Kim, Y.; Kim, B.S.; Gerhardt, F. Comparative study on analysis methods for added resistance of four ships in head and oblique waves. *Ocean Eng.* **2021**, *236*, 109552. [CrossRef]
4. Bessho, M.; Kyozuka, Y.; Miyazaki, M. On the Ship Motion Reduction by Anti-Pitching Fins in Head Seas. *J. Soc. Nav. Archit. Jpn.* **1983**, *153*, 176–187. [CrossRef]

5. Wu, T.N.; Guo, J.; Chen, Y.N.; Chen, W.C. Experimental study of ship pitching motion reduction using anti-pitching fins. In *Proceedings of the JFPS International Symposium on Fluid Power*; The Japan Fluid Power System Society: Tokyo, Japan, 1996; Volume 3, pp. 223–228. [CrossRef]
6. Sclavounos, P.D.; Borgen, H. Seakeeping Analysis of a High-Speed Monohull With a Motion-Control Bow Hydrofoil. *J. Ship Res.* **2004**, *48*, 77–117. [CrossRef]
7. Wu, T. Extraction of flow energy by a wing oscillating in waves. *J. Ship Res.* **1972**, *16*, 66–78. [CrossRef]
8. Isshiki, H. A Theory of Wave Devouring Propulsion (1st Report). *J. Soc. Nav. Archit. Jpn.* **1982**, *151*, 54–64. [CrossRef]
9. Isshiki, H.; Murakami, M. A Theory of Wave Devouring Propulsion (4th Report). *J. Soc. Nav. Archit. Jpn.* **1984**, *156*, 102–114. [CrossRef]
10. Isshiki, H.; Murakami, M.; Terao, Y. *Thrust Generation by a Hydrofoil Driven by Waves-A Basic Aspect of Wave Devouring Propulsion*; Springer: Berlin/Heidelberg, Germany, 1986.
11. Grue, J.; Mo, A.; Palm, E. Propulsion of a foil moving in water waves. *J. Fluid Mech.* **1988**, *186*, 393–417. [CrossRef]
12. Jakobsen, E. The foil propeller, wave power for propulsion. In *2nd International Symposium on Wave and Tidal Energy*; BHRA Fluid Engineering: Cranfield, UK, 1981; pp. 363–369.
13. Naito, S.; Isshiki, H.; Fujimoto, K. Thrust generation of a fin attached to a ship in waves. *J. Kansai Soc. Nav. Archit.* **1986**, *202*, 23–29.
14. Zhang, Y.P.; Xu, L. A propulsion unit for ships based on water-treading of flapping foils. *Ocean Eng.* **2021**, *235*, 109330. [CrossRef]
15. Zhang, Y.P.; Xu, L.; Zhou, Y. A wave foil with passive angle of attack adjustment for wave energy extraction for ships. *Ocean Eng.* **2022**, *246*, 110627. [CrossRef]
16. Rozhdestvensky, K.V.; Htet, Z.M. A mathematical model of a ship with wings propelled by waves. *J. Mar. Sci. Appl.* **2021**, *20*, 595–620. [CrossRef]
17. Bøckmann, E.; Steen, S. Model test and simulation of a ship with wavefoils. *Appl. Ocean Res.* **2016**, *57*, 8–18. [CrossRef]
18. Linden, H. Improved Combination with Floating Bodies, of Fins Adapted to Effect Their Propulsion. GB Patent GBD189514630, 18 July 1896.
19. Rozhdestvensky, K.V.; Ryzhov, V.A. Aerohydrodynamics of flapping-wing propulsors. *Prog. Aerosp. Sci.* **2003**, *39*, 585–633. [CrossRef]
20. Naito, S.; Isshiki, H. Effect of bow wings on ship propulsion and motions. *Appl. Mech. Rev.* **2005**, *58*, 253–268. [CrossRef]
21. Terao, Y. Wave devouring propulsion system—From concept to trans-pacific voyage. In Proceedings of the International Conference on Offshore Mechanics and Arctic Engineering—OMAE. American Society of Mechanical Engineers Digital Collection, Honolulu, HI, USA, 31 May–5 June 2009; pp. 119–126.
22. Terao, Y.; Sakagami, N. Design and development of an autonomous wave-powered boat with a wave devouring propulsion system. *Adv. Robot.* **2015**, *29*, 89–102. [CrossRef]
23. Bøckmann, E.; Steen, S. Experiments with actively pitch-controlled and spring-loaded oscillating foils. *Appl. Ocean Res.* **2014**, *48*, 227–235. [CrossRef]
24. Bowker, J.A.; Tan, M.; Townsend, N.C. Forward speed prediction of a free-running wave-propelled boat. *IEEE J. Ocean. Eng.* **2020**, *46*, 402–413. [CrossRef]
25. Bowker, J.A.; Townsend, N.C. Evaluation of bow foils on ship delivered power in waves using model tests. *Appl. Ocean Res.* **2022**, *123*, 103148. [CrossRef]
26. De Silva, L.W.A.; Yamaguchi, H. Numerical study on active wave devouring propulsion. *J. Mar. Sci. Technol.* **2012**, *17*, 261–275. [CrossRef]
27. Politis, G.K.; Politis, K. Biomimetic propulsion under random heaving conditions, using active pitch control. *J. Fluid Struct.* **2014**, *47*, 139–149. [CrossRef]
28. Belibassakis, K.; Politis, G. Hydrodynamic performance of flapping wings for augmenting ship propulsion in waves. *Ocean Eng.* **2013**, *72*, 227–240. [CrossRef]
29. Belibassakis, K.; Filippas, E. Ship propulsion in waves by actively controlled flapping foils. *Appl. Ocean Res.* **2015**, *52*, 1–11. [CrossRef]
30. Filippas, E.S. Augmenting Ship Propulsion in Waves Using Flapping Foils Initially Designed for Roll Stabilization. *Procedia Comput. Sci.* **2015**, *66*, 103–111. [CrossRef]
31. Huang, S.W.; Wu, T.L.; Hsu, Y.T.; Guo, J.H.; Tsai, J.F.; Chiu, F.C. Effective energy-saving device of eco-ship by using wave propulsion. In Proceedings of the 2016 Techno-Ocean (Techno-Ocean), Kobe, Japan, 6–8 October 2016.
32. Filippas, E.S.; Belibassakis, K.A. A nonlinear time-domain BEM for the performance of 3D flapping-wing thrusters in directional waves. *Ocean Eng.* **2022**, *245*, 110157. [CrossRef]
33. Belibassakis, K.; Filippas, E.; Papadakis, G. Numerical and Experimental Investigation of the Performance of Dynamic Wing for Augmenting Ship Propulsion in Head and Quartering Seas. *J. Mar. Sci. Eng.* **2022**, *10*, 24. [CrossRef]
34. Feng, P.; Ma, N.; Gu, X. A practical method for predicting the propulsive performance of energy efficient ship with wave devouring hydrofoils at actual seas. *Proc. Inst. Mech. Eng. Part M J. Eng. Marit. Environ.* **2014**, *228*, 348–361. [CrossRef]
35. Bøckmann, E.; Yrke, A.; Steen, S. Fuel savings for a general cargo ship employing retractable bow foils. *Appl. Ocean Res.* **2018**, *76*, 1–10. [CrossRef]

36. Filippas, E.S.; Belibassakis, K.A. Hydrodynamic analysis of flapping-foil thrusters operating beneath the free surface and in waves. *Eng. Anal. Bound. Elem.* **2014**, *41*, 47–59. [CrossRef]
37. Politis, G.K. A BEM code for the calculation of flow around systems of independently moving bodies including free shear layer dynamics. In Proceedings of the Advances Boundary Elemen Techniques X, WIT Conference, Athens, Greece, 9–11 July 2008.
38. Wilson, R.V.; Stern, F.; Coleman, H.W.; Paterson, E.G. Comprehensive Approach to Verification and Validation of CFD Simulations part 2: Application for Rans Simulation of a Cargo/Container Ship. *J. Fluids Eng.* **2001**, *123*, 803–810. [CrossRef]
39. Simone, M.; Ermina, B.; Day, A.H.; Atilla, I. Verification and validation of numerical modelling of dtmb 5415 roll decay. *Ocean Eng.* 2018; 162, 209–223.
40. Bhushan, S.; Yoon, H.; Stern, F. Detached eddy simulations and tomographic piv measurements of flows over surface combatant 5415 at straight-ahead and static drift conditions. *Ocean Eng.* **2021**, *238*, 109658. [CrossRef]
41. Anderson, J.M.; Streitlien, K.; Barrett, D.S.; Triantafyllou, M.S. Oscillating foils of high propulsive efficiency. *J. Fluid Mech.* **1998**, *360*, 41–72. [CrossRef]
42. Read, D.A.; Hover, F.S.; Triantafyllou, M.S. Forces on oscillating foils for propulsion and maneuvering. *J. Fluid Struct.* **2003**, *17*, 163–183. [CrossRef]
43. Schouveiler, L.; Hover, F.S.; Triantafyllou, M.S. Performance of flapping foil propulsion. *J. Fluid Struct.* **2005**, *20*, 949–959. [CrossRef]
44. Thaweewat, N.; Phoemsapthawee, S.; Juntasaro, V. Semi-active flapping foil for marine propulsion. *Ocean Eng.* **2018**, *147*, 556–564. [CrossRef]
45. Mei, L.; Yan, W.; Zhou, J.; Yu, D.; Wu, P. Working characteristics of self-pitching flapping foil propulsor. In the 9th Conference on Computational Methods in Marine Engineering; Marine: 2021; Edinburgh. [CrossRef]
46. Mei, L.; Zhou, J.; Dong, Y.; Shi, W.; Pan, X.; Li, M. Parametric Analysis for Underwater Flapping Foil Propulsor. *Water* **2021**, *13*, 2103. [CrossRef]
47. Zhou, J.; Yan, W.; Mei, L.; Cong, L.; Shi, W. Principal Parameters Analysis of the Double-Elastic-Constrained Flapping Hydrofoil for Tidal Current Energy Extraction. *J. Mar. Sci. Eng.* **2022**, *10*, 855. [CrossRef]
48. Duvigneau, R.; Visonneau, M. On the role played by turbulence closures in hull shape optimization at model and full scale. *J Mar. Sci. Technol.* **2003**, *8*, 11–25. [CrossRef]
49. Queutey, P.; Visonneau, M. An interface capturing method for free-surface hydrodynamic flows. *Comput. Fluids* **2007**, *36*, 1481. [CrossRef]
50. Rhie, C.M. Numerical study of the turbulent flow past an isolated airfoil with trailing edge separation. *AIAA J.* **1983**, *21*, 1525–1532. [CrossRef]
51. Jasak, H. Error Analysis and Estimation for the Finite Volume Method with Applications to Fluid Flows. Ph.D. Thesis, University of London, London, UK, 1996.
52. Muzaferija, S.; Peric, M. Computation of free surface flows using interface-tracking and interface-capturing methods. In *Nonlinear Water Wave Interaction*; Mahrenholtz, O., Markiewicz, M., Eds.; WIT Press: Southampton, UK, 1999; ; pp. 59–100.
53. Olivieri, A.; Pistani, F.; Avanzini, A.; Stern, F.; Penna, R. *Towing Tank Experiments of Resistance, Sinkage and Trim, Boundary Layer, Wake, and Free Surface Flow Around a Naval Combatant Insean 2340 Model*; College of Engineering: Iowa City, IA, USA, 2001; p. 42.
54. Irvine, M. Pitch and Heave Tests and Uncertainty Assessment for a Surface Combatant in Regular Head Waves. *J. Ship. Res.* **2008**, *52*, 146–163. [CrossRef]
55. Gui, L.; Longo, J.; Metcalf, B.; Shao, J.; Stern, F. Forces, moment, and wave pattern for surface combatant in regular head wavesPart I. Measurement systems and uncertainty assessment. *Exp. Fluids.* **2001**, *31*, 674–680. [CrossRef]
56. Wang, Z.D.; Lao, Y.J.; Li, L.J.; Cong, W.C. Experiment on the characteristics of 3-d vortex ring behind a flexible oscillating caudal fin. *J. Hydrodyn.* **2010**, *22*, 393–401. [CrossRef]
57. Buchholz, J.H.J.; Smits, A.J. On the evolution of the wake structure produced by a low-aspect-ratio pitching panel. *J. Fluid Mech.* **2006**, *564*, 433–443. [CrossRef] [PubMed]
58. Terao, Y.; Isshiki, H. Wave devouring propulsion sea trial. In *Eighteenth Symposium on Naval Hydrodynamics*; Seaworthiness: Washington, DC, USA, 1991; pp. 296–297.
59. Triantafyllou, G.S.; Gopalkrishnan, R. Wake mechanics for thrust generation in oscillating foils. *Phys. Fluids* **1991**, *3*, 2835–2837. [CrossRef]